Geochimica et Cosmochimica Acta 417 (2026) 211–229

Contents lists available at ScienceDirect

Geochimica et Cosmochimica Acta

journal homepage: www.elsevier.com/locate/gca

Contrasting coprecipitation and recrystallization mechanisms for Ra immobilization via (Ba,Ra)SO_4 solid solution formation in fractured crystalline rocks: Insights from 3D reactive transport modeling

Yumeng Wang [a,*], Peter Alt-Epping [b], Guido Deissmann [a], Yuankai Yang [a], Jun Hu [c], Dirk Bosbach [a], Jenna Poonoosamy [a]

[a] Institute of Fusion Energy and Nuclear Waste Management (IFN-2), Forschungszentrum Jülich GmbH, Jülich 52428, Germany
[b] Institute of Geological Sciences, University of Bern, Bern CH-3012, Switzerland
[c] Department of Civil and Environmental Engineering, Princeton University, Princeton 08544, United States

ARTICLE INFO

Associate editor: Christophe Tournassat

Keywords:
3D reactive transport
Solid solutions
Radium
Coprecipitation
Recrystallization
Coupled dissolution-reprecipitation
Reaction kinetics
Fracture-matrix systems
Nuclear waste disposal

ABSTRACT

Ra incorporation into (Ba,Ra)SO_4 solid solutions is a key control on Ra mobility in groundwater systems and typically occurs through coprecipitation and recrystallization. The effectiveness and persistence of these mechanisms under long-term reactive transport conditions remain poorly constrained, particularly in fractured crystalline rocks, where Ra migration is controlled by the coupled effects of heterogeneous flow, advective–diffusive transport, fracture-matrix mass exchange, reaction kinetics, and evolving hydrogeochemical conditions. Here, we employ 3D reactive transport modeling using PFLOTRAN to investigate Ra mobility under near-field conditions relevant to geological nuclear waste repositories. The models couple fluid flow, solute transport, and non-ideal solid solution-aqueous solution (SS-AS) interactions, incorporating a regular Guggenheim solid solution model and composition-dependent dissolution-precipitation kinetics for stoichiometric solid solutions. Simulations are conducted in a 10 m × 10 m × 10 m fracture-matrix domain upscaled from a discrete fracture network, with a constant-flux inflow boundary and fixed Ra concentration representing a sustained Ra source over 10,000 years. The results show that coprecipitation leads to strong but transient Ra immobilization, with substantial Ra uptake within the first ~200 years, followed by progressive Ra remobilization as sulfate is depleted and previously formed solid solutions dissolve. Consequently, Ra retention decreases markedly and becomes minimal after ~1000 years. In contrast, recrystallization supports persistent Ra immobilization throughout the entire 10,000-year simulation period, provided that sufficient barite remains available within fracture zones. This mechanism is sustained by kinetically controlled coupled dissolution-reprecipitation and produces a characteristic spatial zonation, with Ra-rich solid solutions near inflow regions and progressively Ba-rich compositions downstream. Sensitivity analyses further demonstrate that increasing Ba/Ra ratios in the inflowing fluid can reduce the long-term Ra retention under kinetically controlled reactive transport conditions, in contrast to predictions based solely on thermodynamic equilibrium. Fractures are identified as the dominant domains for long-term Ra immobilization, whereas the low-permeability matrix contributes only minimally due to limited diffusive accessibility. Once fractures lose their retention capacity, aqueous Ra is predominantly flushed from the system rather than retained within the matrix. Overall, these results suggest that equilibrium assumptions commonly adopted in radionuclide safety assessments are insufficient to predict Ra behavior in complex subsurface systems, and thus robust evaluation of long-term Ra mobility requires coupling reaction mechanisms and kinetics with flow and transport in evolving fracture-matrix systems. Although both coprecipitation and recrystallization form (Ba,Ra)SO_4 solid solutions, their distinct microscopic mechanisms lead to contrasting long-term behaviors when upscaled to the field scale. These findings have important implications for nuclear waste disposal and managing Ra contamination in geothermal and mining environments.

* Corresponding author.
E-mail address: geomeng@foxmail.com (Y. Wang).

https://doi.org/10.1016/j.gca.2026.01.045
Received 1 October 2025; Accepted 28 January 2026
Available online 2 February 2026

1. Introduction

The mobility of trace elements in groundwater is fundamental to ore deposit formation, contaminant migration, and safe disposal of nuclear waste (White, 2020; Rollinson and Pease, 2021). A primary process limiting their mobility is sorption onto mineral surfaces, which typically represents the first mechanism retarding their transport in water–rock systems (Langmuir, 1997; Bethke, 2022). Sorption, principally through ion exchange and surface complexation, is particularly effective for certain trace elements (e.g., actinides) in lithologies with high sorption capacities (e.g., clays), and its efficiency is controlled by mineral surface area, pH, ionic strength, and the presence of competing ions (Tournassat et al., 2013; Bethke, 2022). However, sorption is intrinsically inefficient for some elements. For instance, radium (Ra), as a divalent cation with a large ionic radius, is only weakly retained in lithologies with limited sorption capacity, such as crystalline rocks (Fernandes et al., 2023; Fabritius et al., 2024). Under such conditions, incorporation into thermodynamically stable mineral lattices via solid solution formation becomes the dominant mechanism for long-term immobilization (Prieto, 2009; Vinograd et al., 2018). This process occurs within a wide range of mineral groups, including carbonates (Tesoriero and Pankow, 1996), phosphates (Kersten, 2025), silicates (Tutolo and Leong, 2025), and sulfates (Glynn, 2000), and therefore plays a vital role in controlling the fate of radionuclides, whose mobility over geological timescales poses radiological hazards and presents major challenges for safety assessment and remediation strategies (Bosbach et al., 2020).

Ra is a naturally occurring radionuclide produced by the decay of ^{238}U and ^{232}Th. Its most abundant isotope, ^{226}Ra, is highly radiotoxic with a half-life of ~1600 years (Langmuir and Riese, 1985). In radioactive waste, Ra becomes increasingly important over time (up to 10^6 years), as it is continuously generated by the decay of UO_2 spent fuel, and unlike many short-lived fission products, persists as a major long-term contributor to radiological dose (SKB, 2011). The formation of $(Ba,Ra)SO_4$ solid solutions is widely regarded as the primary mechanism controlling Ra transport in groundwater systems (Zhu, 2004; Vinograd et al., 2013). This is because $(Ba,Ra)SO_4$ solid solutions are significantly less soluble than pure $RaSO_4$, thereby maintaining aqueous Ra concentrations well below $RaSO_4$ saturation (Berner and Curti, 2002; Bosbach et al., 2010; Curti et al., 2010; Klinkenberg et al., 2014; Brandt et al., 2015,2020). Increasing Ba/Ra ratios further decrease Ra solubility through the so-called "dilution effect" (Fig. 1A). This effect is widely invoked to explain the low Ra concentrations observed in natural waters and constitutes a key assumption in safety assessment of Ra migration potential in near-field environments of geological repositories (Fig. 1B; Grandia et al., 2008; Vinograd et al., 2013).

Mechanistically, $(Ba,Ra)SO_4$ solid solutions can form via coprecipitation and recrystallization (Fig. 1C). Coprecipitation occurs when fluids become supersaturated with respect to $(Ba,Ra)SO_4$, typically due to mixing between Ba/Ra-bearing and sulfate-bearing fluids or through evaporation. In contrast, recrystallization involves the progressive incorporation of Ra into pre-existing barite through coupled dissolution–reprecipitation processes (Fig. 1C). Evidence for coprecipitation has been reported in various natural and engineered environments, including evaporitic deposits (Rosenberg et al., 2018; Zhang et al., 2025), geothermal pipe scaling (Fisher, 1998), uranium and coal mining sites (Liu and Hendry, 2011; Jirásek et al., 2020), hydrocarbon production systems (Zhang et al., 2014), and wastewater treatment facilities (IAEA, 2003). Coprecipitation is also relevant to nuclear waste repositories, where Ba and Ra may be co-released from waste and subsequently interact with sulfate-bearing formation waters (Grandia et al., 2008; Curti et al., 2019; Ait-Mouheb et al., 2024). By contrast, recrystallization is expected to dominate under conditions where pre-existing

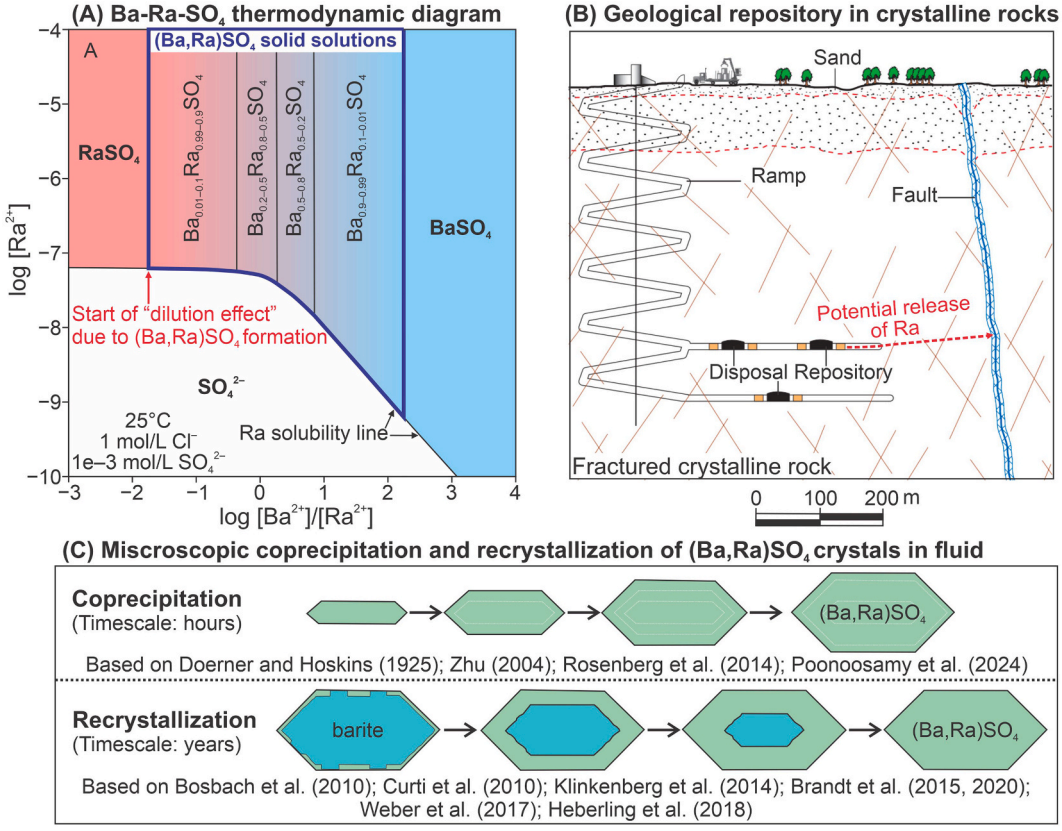

Fig. 1. (A) Thermodynamic predominance diagram of the Ba-Ra-SO_4 system showing a decrease in Ra solubility with increasing Ba^{2+}/Ra^{2+} activity ratios. (B) Conceptual illustration of a geological repository in fractured crystalline rocks, highlighting potential Ra release and transport along fracture networks. (C) Schematic illustration of microscopic coprecipitation and recrystallization processes leading to the formation of $(Ba,Ra)SO_4$ solid solutions.

barite interacts with Ra-bearing fluids derived from the decay of long-lived ^{238}U in spent fuel. Barite initially precipitated from Ba-bearing fluids associated with the decay of short-lived Cs-isotopes (e.g., ^{137}Cs, ^{134}Cs) may form before Ra release and subsequently incorporate Ra through recrystallization (Curti et al., 2010; Klinkenberg et al., 2014; Brandt et al., 2015,2020). This mechanism also occurs in natural aquifers and has been employed in engineered remediation strategies, where barite has been used as a reactive barrier to immobilize Ra in mining effluents (Jirásek et al., 2020; Besançon et al., 2025).

Previous studies have constrained both the thermodynamic and kinetic properties of the Ba-Ra-SO_4 system. For example, the non-ideal mixing behavior of (Ba,Ra)SO_4 solid solutions has been described using Guggenheim interaction parameters derived from quantum mechanical calculations (Vinograd et al., 2013, 2018). Precipitation rate constants have been constrained through microfluidic experiments (Poonoosamy et al., 2024), batch studies (Hedström et al., 2013), and atomistic simulations (Rudin et al., 2024). Laboratory observations consistently show that coprecipitation proceeds rapidly, typically on timescales of hours (Rosenberg et al., 2014, 2018; Poonoosamy et al., 2024), whereas recrystallization is markedly slower, requiring years to achieve complete replacement (Bosbach et al., 2010; Curti et al., 2010; Klinkenberg et al., 2014; Brandt et al., 2015,2020; Heberling et al., 2018; Fig. 1C). However, applying such parameters to natural subsurface systems remains challenging because geochemical reactions are tightly coupled with flow and transport processes in heterogeneous geological media (Steefel et al., 2005,2015). Although Ra reactive transport has been investigated using 1D continuum-scale models (Shao et al., 2009) and pore-scale simulations based on the Lattice Boltzmann method (Curti et al., 2019), the roles of fracture-matrix systems in controlling Ra immobilization remains poorly constrained. This gap is critical because fractured crystalline rocks host, or are planned to host, nuclear waste repositories (e.g., in Finland, Sweden, and Canada; Hedin and Olsson, 2016), as well as groundwater and geothermal resources (Coleman et al., 2015), all of which are relevant to Ra contamination issues.

Fractures are widely recognized as the dominant pathways for flow and transport in crystalline rocks (Viswanathan et al., 2021; Steefel and Hu, 2022; Andrews et al., 2023), whereas the adjacent low-permeability matrix is commonly regarded as the primary domain for long-term radionuclide immobilization by matrix diffusion (Zuber and Motyka, 1994, MacQuarrie and Mayer, 2005; Tsang et al., 2015; Zhang et al., 2022; Yang et al., 2024). Field tests at the Grimsel Underground Laboratory in Switzerland support this conventional viewpoint, demonstrating rapid advective transport along fracture networks and slow solute exchange with the surrounding matrix (Dideriksen et al., 2010). However, because these experiments span only a few years, they cannot capture long-term water–rock interactions and may therefore underestimate the significance of fracture networks for radionuclide immobilization. Consequently, the relative contributions of fractures and the matrix to long-term Ra immobilization remain poorly constrained. This uncertainty is critical, as fracture networks can act not only as transport pathways but also as highly reactive environments that promote Ra immobilization via coprecipitation or recrystallization, as evidenced by the widespread occurrence of mineral-filled veins and fault systems in crystalline rocks (Bons et al., 2012; Wang et al., 2024).

Taken together, this study aims to address three key questions: (1) how coprecipitation and recrystallization control the spatiotemporal distribution of (Ba,Ra)SO_4 solid solutions and long-term Ra immobilization in fracture-matrix systems under dynamic reactive flow transport; (2) whether the thermodynamically predicted “dilution effect” persists when solid solution-aqueous solution (SS-AS) interactions are kinetically controlled in natural flow conditions; and (3) which hydrogeochemical factors control Ra immobilization in fractures versus the matrix over short- and long-term timescales. To address these questions, we employ 3D reactive transport modeling that couples heterogeneous flow and solute transport with kinetically controlled, non-ideal SS-AS interactions in fracture-matrix systems. The modeling framework integrates upscaled discrete fracture-matrix (UDFM) models derived from discrete fracture networks (DFN) (Hyman et al., 2015; Sweeney et al., 2020) with massively parallel PFLOTRAN simulations on high-performance computers (Hammond et al., 2013; Lichtner et al., 2015). Our results demonstrate that coprecipitation and recrystallization have contrasting controls on long-term Ra mobility in fractured crystalline rocks, with Ra immobilization controlled by the coupled effects of reaction mechanisms, kinetics, and fracture-matrix hydrogeology. These findings provide a mechanistic basis for predicting long-term Ra behavior in geological nuclear waste disposal systems, enhanced geothermal systems, and groundwater resources, and provide new insights into mineralization processes of critical trace metal deposits in complex subsurface environments.

2. Methods

2.1. Modeling overview

We conducted 3D reactive transport modeling and thermodynamic reaction path modeling to investigate the formation of (Ba,Ra)SO_4 solid solutions and their impact on Ra transport in fractured crystalline rocks. Reaction path models were calculated independently using PHREEQC (Parkhurst and Appelo, 1999) to quantify SS-AS equilibrium conditions over a range of fluid/solid mass ratios. These calculations account for non-ideal solid solution behavior based on endmember solubility products and Guggenheim interaction parameters and are used here to establish equilibrium reference trends and the “dilution effect”. Reactive transport modeling was performed using PFLOTRAN (Hammond et al., 2013; Lichtner et al., 2015), a massively parallel code that solves coupled flow, transport and geochemical reaction equations using a finite volume method and Newton-Krylov iteration. In PFLOTRAN, (Ba, Ra)SO_4 solid solutions are represented as a set of discretized stoichiometric phases governed by kinetic precipitation-dissolution rate laws. Discrete fracture networks (DFN) were generated using DFNWORKS (Hyman et al., 2014,2015) and upscaled to continuum representations through the Upscaled Discrete Fracture Matrix (UDFM) approach, enabling simulation of heterogeneous fracture-matrix flow and fracture-matrix interactions and their control on Ra mobility (Sweeney et al., 2020).

2.2. Geochemical models for solid solution-aqueous solution (SS-AS) interactions

Two modeling approaches are commonly used to describe SS-AS equilibrium conditions. The first treats solid solutions as continuous phases and determines equilibrium by minimizing the Gibbs free energy of the entire system, as implemented in the GEM-Selektor (GEMS) code (Kulik et al., 2013). This approach is thermodynamically rigorous and particularly well suited for equilibrium modeling of complex SS-AS systems, such as non-ideal ternary (Ba,Sr,Ra)SO_4 solid solutions (Vinograd et al., 2018). However, coupling GEMS with flow and transport solvers remains computationally prohibitive for long-term, 3D reactive transport modeling in fracture-matrix systems, and existing applications are largely limited to simplified 1D or 2D models (Kosakowski and Watanabe, 2014). The second approach represents solid solutions as a finite set of discrete stoichiometric endmembers based on the law of mass action method (Reed, 1982). Precipitation and dissolution of these endmembers are governed by stoichiometric solubility products (Glynn et al., 1990). This formulation is computationally efficient and readily coupled with kinetic rate laws, making it well suited for reactive transport modeling in complex geological systems. A recognized limitation of this approach is that equilibrium solid solution compositions must be specified by the users. If the endmembers are not appropriately selected, the system may evolve toward a metastable state in equilibrium with other specified phases rather than toward true

thermodynamic equilibrium (Prieto, 2009). This limitation can be mitigated by approximating a continuous solid solution using a set of kinetically formulated stoichiometric endmembers spanning the relevant compositional range (Lichtner and Carey, 2006). Under this formulation, thermodynamically unstable phases preferentially dissolve, whereas more stable compositions precipitate, enabling a self-organized evolution toward equilibrium through coupled dissolution-reprecipitation processes (Lichtner and Carey, 2006).

Following the approach of Lichtner and Carey (2006), this study represents (Ba,Ra)SO_4 solid solutions as a finite set of stoichiometric phases that precipitate and dissolve kinetically. Potential Sr incorporation leading to ternary (Ba,Sr,Ra)SO_4 solid solutions is not considered. Dissolution and precipitation rates are described using Transition State Theory (TST):

$$R_m = -A_m \bullet k_{ml} \bullet |1 - \Omega_{st}|^{\beta_m} \bullet \mathrm{sign}(1 - \Omega_{st}) \quad (1)$$

where R_m is the reaction rate (mol•m^{-3}•s^{-1}), A_m the specific surface area (m^{-1}), k_{ml} the intrinsic rate constant (mol•m^{-2}•s^{-1}), β_m the affinity exponent, and Ω_{st} the stoichiometric supersaturation ratio. These parameters are either user-defined or dynamically updated during simulations, enabling precipitation-dissolution kinetics to evolve with solid solution composition and local under- or supersaturation conditions (Lichtner and Carey, 2006).

Thermodynamic SS-AS equilibrium is described using the law of mass action, with solid-phase activity coefficients accounting for non-ideal mixing between the pure $BaSO_4$ and $RaSO_4$ endmembers (Prieto, 2009):

$$a_{Ba^{2+}} \bullet a_{SO_4^{2-}} = K_{BaSO_4} X_{BaSO_4} \gamma_{BaSO_4} \quad (2)$$

$$a_{Ra^{2+}} \bullet a_{SO_4^{2-}} = K_{RaSO_4} X_{RaSO_4} \gamma_{RaSO_4} \quad (3)$$

where a_i denotes aqueous activity of species i, X_j the mole fraction of pure endmember j in the solid solution, K_j the solubility product of the pure endmember, and γ_j the corresponding solid-phase activity coefficient, which is described using a regular solid solution model:

$$\ln\gamma_{BaSO_4} = G_0(1 - X_{BaSO_4})^2 \quad (4)$$

$$\ln\gamma_{RaSO_4} = G_0(1 - X_{RaSO_4})^2 \quad (5)$$

where the Guggenheim interaction parameter G_0 is set to 1 (Vinograd et al., 2013). Solubility products of the pure endmembers are $\log K_{RaSO_4} = -10.26$ (Langmuir and Riese, 1985) and $\log K_{BaSO_4} = -9.97$ (Johnson et al., 1992). These parameters were used to construct a Lippmann diagram illustrating SS-AS equilibrium relationships (Fig. 2A).

To represent equilibrium conditions for stoichiometric solid solutions, we introduce the stoichiometric solubility product (K_{st}), which is analogous to the solubility product (K_{sp}) of a pure phase but applies to non-ideal stoichiometric solid solutions (e.g., $Ba_xRa_{1-x}SO_4$). Each

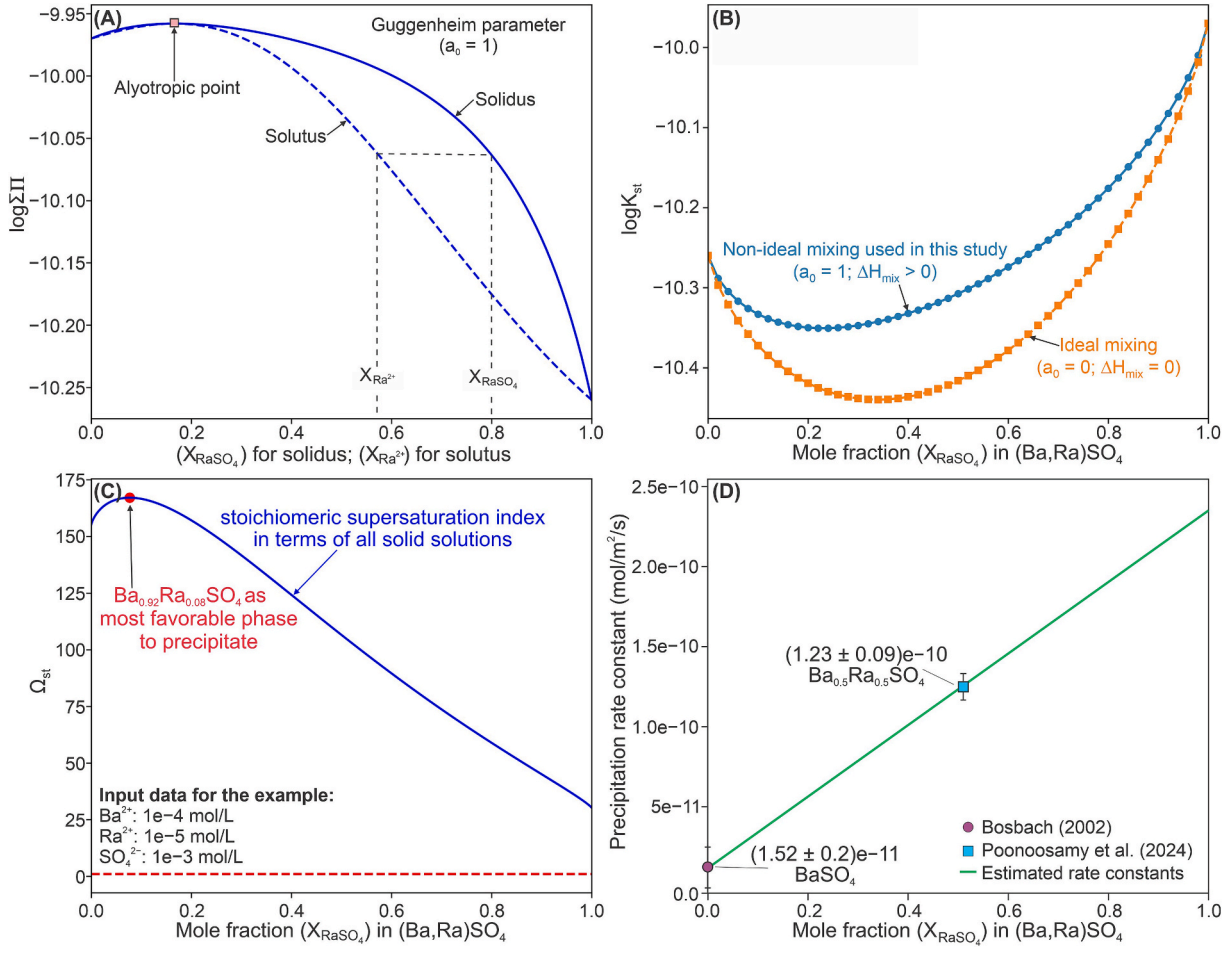

Fig. 2. (A) Lippmann diagram of the (Ba,Ra)SO_4 solid solution-aqueous solution system with a Guggenheim interaction parameter $a_0 = 1$. (B) Stoichiometric solubility product (K_{st}) of (Ba,Ra)SO_4 solid solutions as a function of composition, comparing non-ideal mixing ($a_0 = 1$) and ideal mixing ($a_0 = 0$). (C) Stoichiometric supersaturation ratio (Ω_{st}) of (Ba,Ra)SO_4 solid solutions under conditions of 1×10^{-4} mol/L Ba^{2+}, 1×10^{-5} mol/L Ra^{2+}, and 1×10^{-3} mol/L SO_4^{2-}. (D) Precipitation rate constants for (Ba,Ra)SO_4 solid solutions estimated from experimental kinetic data for barite (Bosbach, 2002) and $Ba_{0.5}Ra_{0.5}SO_4$ (Poonoosamy et al., 2024).

stoichiometric solid solution is treated as a single-component phase with a fixed composition that dissolves congruently (Prieto, 2009):

$$Ba_xRa_{1-x}SO_4 \leftrightarrow xBa^{2+} + (1-x)Ra^{2+} + SO_4^{2-} \quad (6)$$

Assuming unit activity of the solid phase, applying the law of mass action yields the stoichiometric solubility product:

$$K_{st} = (a_{Ba^{2+}})^x (a_{Ra^{2+}})^{1-x} a_{SO_4^{2-}} \quad (7)$$

Substituting the endmember equilibrium expressions (Eqs. (2)–(3)) into Eq. (7) yields:

$$K_{st} = (K_{BaSO_4}\gamma_{BaSO_4}X_{BaSO_4})^{X_{Baso_4}} (K_{RaSO_4}\gamma_{RaSO_4}X_{RaSO_4})^{X_{Raso_4}} \quad (8)$$

K_{st} values were pre-calculated over the full range of stoichiometric compositions and incorporated into the thermodynamic database, with details provided in Supplementary Material (SM) Table S1. To evaluate the saturation state of each stoichiometric solid solution during simulations, the stoichiometric saturation ratio (Ω_{st}) is defined as:

$$\Omega_{st}(X_{Ra}) = \frac{IAP_{st}}{K_{st}} = \frac{(a_{Ra^{2+}})^{X_{RaSO_4}} (a_{Ba^{2+}})^{X_{BaSO_4}} (a_{SO_4^{2-}})}{(K_{BaSO_4}\gamma_{BaSO_4}X_{BaSO_4})^{X_{Baso_4}} (K_{RaSO_4}\gamma_{RaSO_4}X_{RaSO_4})^{X_{RaSO_4}}} \quad (9)$$

where IAP_{st} is the stoichiometric ion activity product. Analogous to the classical saturation ratio for a pure phase ($\Omega = IAP/K_{sp}$), $\Omega_{st} > 1$ indicates supersaturation favoring precipitation, $\Omega_{st} < 1$ indicates undersaturation favoring dissolution, and $\Omega_{st} = 1$ corresponds to stoichiometric equilibrium. When multiple stoichiometric solid solutions coexist, the composition associated with the highest Ω_{st} (>1) is thermodynamically favored, and other solid solutions tend to dissolve and reprecipitate toward this composition (Fig. 2C).

Aqueous activity coefficients were calculated using the extended Debye-Hückel B-dot model. Intrinsic precipitation rate constants for (Ba, Ra)SO_4 solid solutions (Eq. (1)) were linearly interpolated between experimentally determined values for barite (1.5×10^{-11} mol•m^{-2}•s^{-1}; Bosbach, 2002) and $Ba_{0.5}Ra_{0.5}SO_4$ (1.23×10^{-10} mol•m^{-2}•s^{-1}; Poonoosamy et al., 2024) (Fig. 2D; SM Table S2). In the baseline models, dissolution and precipitate rate constants were assumed to be equal, whereas additional sensitivity analyses employed dissolution rate constants three orders of magnitude higher to account for potentially slower nucleation kinetics and elevated saturation thresholds for precipitation (Christy and Putnis, 1993). The continuous (Ba,Ra)SO_4 solid solution was represented using a finite set of stoichiometric phases with non-uniform compositional resolution. Finer discretization was applied toward Ba-rich compositions to capture trace Ra incorporation under highly Ba-dominated conditions, whereas coarser discretization was used toward Ra-rich compositions. Details of the discretization scheme for each model are provided in SM Table S3.

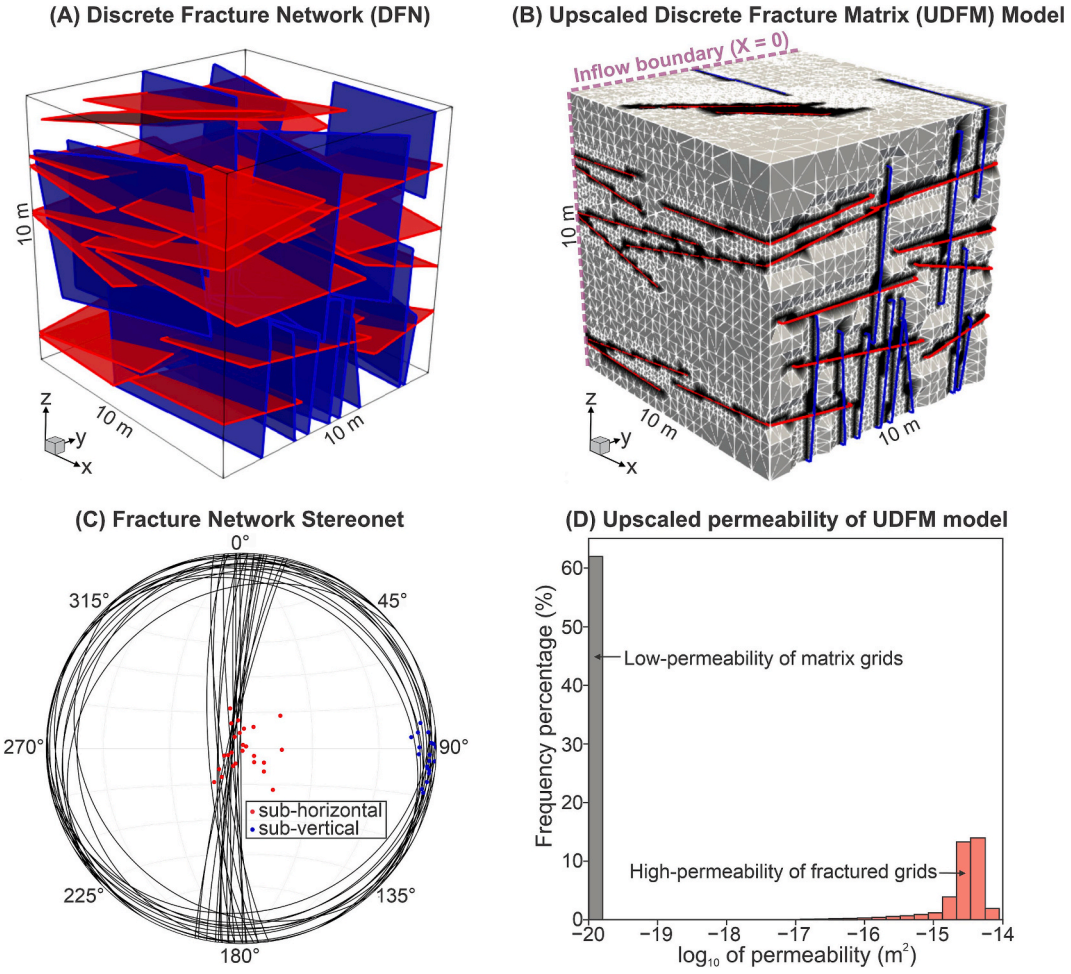

Fig. 3. (A) Discrete fracture network (DFN) model constructed for the crystalline rock domain. (B) Upscaled discrete fracture matrix (UDFM) model used in 3D reactive transport modeling, with the inflow boundary condition indicated. (C) Stereonet of the DFN model showing two dominant fracture sets: sub-horizontal and sub-vertical orientations. (D) Upscaled permeability distribution of the UDFM model, illustrating high-permeability fracture grid cells and low-permeability matrix grid cells.

2.3. 3D reactive transport modeling of Ra retention in fractured crystalline rocks

2.3.1. Conceptual hydrogeologic model

A 10 m × 10 m × 10 m domain was used to represent fractured crystalline rocks in the near-field environments of a geological repository of radioactive waste (Fig. 1B). After the failure of waste canisters, Ra produced by the decay of U^{238} (constituting ~95% of the waste inventory in spent fuel repositories) is mobilized by groundwater and enters the surrounding domain, where it interacts with fractured crystalline rock and is attenuated through (Ba,Ra)SO_4 solid solution formation (Bosbach et al., 2010; SKB, 2011). The DFN comprises 44 planar fractures stochastically distributed according to a 3D von Mises-Fisher distribution (Fig. 3A) and was upscaled into an unstructured UDFM mesh comprising 82,391 unstructured grid cells (Fig. 3B), with locally refined resolution at fracture intersections to capture localized flow and transport. Stereonet analysis indicates two dominant fracture sets, including subhorizontal fractures with low dip angles (0–30°) and subvertical fractures with high dip angles (70–90°), both trending approximately north–south (Fig. 3C). This fracture geometry is consistent with natural fracture networks in crystalline bedrock sites such as Olkiluoto, Finland (Fox et al., 2012; Eeva et al., 2023), and Forsmark, Sweden (Hedin and Olsson, 2016; Doolaeghe et al., 2023). Fracture permeabilities were assigned from 10^{-16} to 10^{-14} m^2 using a volume averaging scheme (Sweeney et al., 2020), consistent with measurements from naturally fractured granitic rocks (Brace, 1984). The rock matrix was assigned to have a low permeability of 1×10^{-20} m^2 (Fig. 3D), representative of intact crystalline rocks containing only microfractures (Scibek et al., 2025). Porosities were set to 1% for the matrix and 10% for fractures based on laboratory and field data for granitic rocks (Fig. 3D; Schild et al., 2001; Tullborg and Larson, 2006).

2.3.2. Boundary and initial conditions for baseline models

The model domain was defined with an inflow boundary through which Ra-rich groundwater entered the system, while all remaining boundaries were assigned as outflow boundaries that allow fluid to exit naturally (Fig. 3B). A hydrostatic pressure gradient was imposed as the initial condition. The inflow boundary was specified as a Neumann-type condition with a constant influx rate of 0.005 m/yr, consistent with groundwater flow rates in low-permeability crystalline rocks in tectonically stable cratonic settings (Hartley et al., 2004; Freeze et al., 2019). All other boundaries were assigned zero-gradient Neumann conditions for flow. For solute transport, the inflow boundary was set as a Dirichlet condition with a fixed chemical composition representing a constant Ra source, whereas outflow boundaries were assigned zero-gradient Neumann conditions, allowing solutes to leave the domain solely by advection.

Two baseline scenarios were simulated to investigate Ra immobilization via coprecipitation and recrystallization. In the coprecipitation model, the domain initially contained sulfate-rich groundwater but no pre-existing barite. The background fluid represented typical crystalline formation waters (Fritz et al., 1994; Boumaiza et al., 2024), with a pH of 7, an ionic strength of 0.1 mol/L NaCl, a sulfate concentration of 1×10^{-3} mol/L, and low background concentrations of Ba^{2+} and Ra^{2+} of 1×10^{-10} mol/L (Table 1). The inflowing fluid was enriched in Ba^{2+} (1×10^{-4} mol/L) and Ra^{2+} (1×10^{-5} mol/L) but depleted in SO_4^{2-} (1×10^{-10} mol/L; Table 1). Although both fluids were undersaturated with respect to (Ba,Ra)SO_4 solid solutions, their strong compositional contrast promoted coprecipitation of (Ba,Ra)SO_4 at fluid mixing zones. In the baseline recrystallization model, the domain initially contained a small amount of barite. The background fluid was equilibrated with barite at pH 7 and an ionic strength of 0.1 mol/L NaCl, resulting in a sulfate concentration of 1×10^{-3} mol/L, a Ba^{2+} concentration of 1.6×10^{-7} mol/L at the barite solubility limit, and a Ra^{2+} concentration of 1×10^{-10} mol/L (Table 1). The inflowing fluid was enriched in Ra^{2+} (1×10^{-5} mol/L) but depleted in Ba^{2+} (1×10^{-10} mol/L), inducing partial barite dissolution followed by reprecipitation of (Ba,Ra)SO_4 solid solutions within the domain.

Table 1
Initial domain and inflow boundary fluid compositions used in the baseline coprecipitation and recrystallization models for reactive transport modeling.

Input parameters		Coprecipitation model		Recrystallization model	
Primary species	Units	Inflow boundary fluid	Initial domain fluid	Inflow boundary fluid	Initial domain fluid
Na^+	mol/L	0.1	0.1	0.1	0.1
Cl^-	mol/L	0.1	0.1	0.1	0.1
Ba^{2+}	mol/L	1×10^{-4}	1×10^{-10}	1×10^{-10}	1.6×10^{-7}
Ra^{2+}	mol/L	1×10^{-5}	1×10^{-10}	1×10^{-5}	1×10^{-10}
SO_4^{2-}	mol/L	1×10^{-10}	1×10^{-3}	1×10^{-10}	1×10^{-3}

In both baseline models, a fixed specific surface area of 100 m^{-1} was assigned to all mineral phases absent at the start of the simulations but permitted to form, ensuring that kinetically controlled precipitation of newly forming phases and dissolution of metastable phases could proceed under the specified initial and boundary conditions. To quantitatively evaluate Ra immobilization, Ra retention efficiency ($E_{retention}$) was quantified using a mass balance approach:

$$E_{retention} = \frac{M_{Ra-in} - M_{Ra-out}}{M_{Ra-in}}$$

where M_{Ra-in} and M_{Ra-out} denote the cumulative masses of Ra entering and leaving the domain through the boundary, respectively.

2.3.3. Sensitivity analysis (SA)

A series of sensitivity analyses (SA-1 to SA-16) were conducted for both the coprecipitation and recrystallization models by varying one parameter at a time relative to the baseline models. An overview of all sensitivity analyses is provided in Table 2.

3. Results

3.1. Thermodynamic reaction path modeling

Thermodynamic reaction path modeling was conducted by progressively adding barite (up to 1×10^{-2} kg) to 1 kg of Ra-rich fluid to evaluate the coupled evolution of aqueous solution chemistry and solid solution composition under equilibrium conditions. The resulting changes in aqueous Ra^{2+} and Ba^{2+} concentrations, solid solution composition, and aqueous Ba/Ra molar ratios are shown in Fig. 4. With increasing barite addition, aqueous Ba^{2+} concentrations increase, whereas Ra^{2+} concentrations decrease (Fig. 4A–B), accompanied by progressive enrichment of solid solutions in $BaSO_4$ relative to $RaSO_4$ (Fig. 4C–D). Consequently, the aqueous Ba/Ra molar ratio increases monotonically with decreasing fluid/solid mass ratio (Fig. 4E). Increasing the initial SO_4^{2-} concentration from 1×10^{-3} to 1×10^{-2} mol/L reduces dissolved Ba^{2+} and Ra^{2+} concentrations by approximately one order of magnitude (Fig. 4A–B), but has little effect on solid solution compositions (X_{RaSO_4}, X_{BaSO_4}) (Fig. 4C–D) or on aqueous Ba/Ra molar ratios (Fig. 4E). The inverse relationship between aqueous Ba/Ra molar ratios and the $RaSO_4$ mole fraction in the solid solution is illustrated in Fig. 4F, where X_{RaSO_4} decreases from 0.98 to 0.077 as the Ba/Ra ratio increases from 0.1 to 100.

3.2. Reactive transport modeling of the baseline coprecipitation model

The baseline coprecipitation model predicts the evolution of (Ba,Ra)

Table 2
Sensitivity analysis (SA) scenarios used to evaluate the impacts of key parameters on Ra retention in coprecipitation and recrystallization models compared to the corresponding baseline models.

SA ID	Model type	Varied parameter	Baseline value	Modified value	Objective (to evaluate)
SA-1	Coprecipitation	Initial SO_4^{2-} concentration	1×10^{-3} mol/L	1×10^{-2} mol/L	Increased sulfate availability
SA-2	Coprecipitation	Inflowing Ba^{2+} concentration	1×10^{-4} mol/L	1×10^{-3} mol/L	Elevated Ba/Ra molar ratio (100:1)
SA-3	Coprecipitation	Inflow velocity	0.005 m/yr	0.05 m/yr	Accelerated advective transport
SA-4	Coprecipitation	Mineral specific surface area	100 m^{-1}	1000 m^{-1}	Enhanced reaction kinetics
SA-5	Coprecipitation	Mineral specific surface area	100 m^{-1}	0.1 m^{-1}	Strongly reduced reaction kinetics
SA-6	Coprecipitation	Diffusion coefficient	1×10^{-10} m^2/s	1×10^{-9} m^2/s	Enhanced diffusive transport
SA-7	Coprecipitation	Dissolution rate constant	Equal to precipitation	$10^3 \times$ precipitation	Accelerated mineral dissolution
SA-8	Coprecipitation	Inflowing Ra^{2+} concentration	1×10^{-5} mol/L	1×10^{-9} mol/L	Strongly reduced Ra supply
SA-9	Recrystallization	Inflowing Ba^{2+} concentration	1×10^{-10} mol/L	1×10^{-4} mol/L	Elevated Ba/Ra molar ratio (100:1)
SA-10	Recrystallization	Inflow velocity	0.005 m/yr	0.05 m/yr	Accelerated advective transport
SA-11	Recrystallization	Barite content	0.1 vol%	0.001 vol%	Reduced barite availability
SA-12	Recrystallization	Mineral specific surface area	100 m^{-1}	1000 m^{-1}	Enhanced reaction kinetics
SA-13	Recrystallization	Mineral specific surface area	100 m^{-1}	10 m^{-1}	Reduced reaction kinetics
SA-14	Recrystallization	Diffusion coefficient	1×10^{-10} m^2/s	1×10^{-9} m^2/s	Enhanced diffusive transport
SA-15	Recrystallization	Dissolution rate constant	Equal to precipitation	$10^3 \times$ precipitation	Accelerated mineral dissolution
SA-16	Recrystallization	Inflowing Ra^{2+} concentration	1×10^{-5} mol/L	1×10^{-9} mol/L	Strongly reduced Ra supply

SO_4 solid solutions over 10,000 years (Fig. 5), together with spatiotemporal variations in aqueous Ra concentrations and Ba/Ra molar ratios (Fig. 6). The domain is initially saturated with sulfate-rich fluids in both fractures and the matrix. Ba/Ra-bearing fluids with a Ba/Ra molar ratio of 10 continuously enter the system, progressively displacing resident fluids and inducing mixing-driven precipitation followed by dissolution of (Ba,Ra)SO_4 solid solutions.

During the early stage of the simulation (≤500 years), coprecipitation occurs predominantly within fractures due to advective mixing between Ba/Ra-rich inflowing fluids and sulfate-rich resident fluids (Fig. 5A–B). Solid solution volume fractions locally reach ~1×10^{-6}, particularly near fracture intersections. As sulfate becomes progressively depleted near the inflow boundary, previously precipitated solid solutions in fractures begin to dissolve. In contrast, coprecipitation in the adjacent matrix increases as Ba^{2+} and Ra^{2+} diffuse from fractures and mix with sulfate-rich matrix fluids. By ~1000 years, solid solutions initially formed in fractures are largely dissolved, and dissolution fronts extend into the matrix (Fig. 5C). From 2000 to 10,000 years, dissolution continues to propagate deeper into the matrix, while coprecipitation persists only within hydraulically isolated matrix regions distal from fractures, where SO_4^{2-} remains available (Fig. 5D–F). At 10,000 years, (Ba,Ra)SO_4 is preserved only within isolated matrix domains (Fig. 5F).

The spatiotemporal evolution of solid solution distributions is consistent with the corresponding changes in aqueous Ra concentrations and Ba/Ra molar ratios. Between 100 and 1000 years, Ra-rich inflowing fluids progressively displace sulfate-rich resident fluids, initially within fractures and subsequently in the adjacent matrix (Fig. 6A–C). By 10,000 years, this displacement is almost complete throughout the entire domain, and Ba/Ra molar ratios converge toward the inflow value of 10, indicating effective compositional homogenization driven by advective–diffusive transport and fluid mixing (Fig. 6D–F).

3.3. Reactive transport modeling of the baseline recrystallization model

Fig. 7 shows the evolution of (Ba,Ra)SO_4 distributions during barite recrystallization over 10,000 years. The domain is initially saturated with sulfate-rich fluids and equilibrated with pre-existing barite uniformly distributed in fractures and the matrix. Continuous inflow of Ra^{2+}-rich (1×10^{-5} mol/L) and Ba^{2+}-poor (1×10^{-10} mol/L) fluids promotes barite dissolution and subsequent (Ba,Ra)SO_4 reprecipitation, leading to progressive Ra incorporation into the solid phase.

During the early stage (≤1000 years), recrystallization occurs predominantly within fractures, where advective transport dominates, while solid solution formation within the matrix remains negligible (Fig. 7A–C). The volume fractions of (Ba,Ra)SO_4 in fractures increase gradually over time at the expense of barite dissolution. From 2000 to 10,000 years, recrystallization remains largely confined to fractures, with peak volume fractions reaching ~1×10^{-3} near the inflow boundary and decreasing downstream (Fig. 7D–F). The overall spatial pattern remains similar to that observed at earlier times, indicating sustained accumulation of solid solutions within fracture zones and only minor recrystallization in the matrix.

The total amount of solid solutions within the domain increases continuously over time, and solid phases spanning a wide range of Ra contents coexist, forming a pronounced zonation pattern in which Ra-rich solid solutions dominate near the inflow boundary, whereas Ra-poor phases prevail downstream. Spatial distributions of aqueous Ra concentrations and Ba/Ra molar ratios delineate finger-shaped reaction fronts within the fracture network (Fig. 8A–F). These fronts are geometrically controlled by fracture orientation and extend slightly into the adjacent matrix, producing sharp geochemical gradients at fracture-matrix interfaces. Aqueous Ra concentrations decrease progressively along the flow path from ~1×10^{-5} mol/L at the inflow boundary to ~1×10^{-10} mol/L downstream, reflecting progressive Ra removal from the aqueous phases and its incorporation into solid solutions by recrystallization. Although the reaction front migrate slowly downstream, its overall geometry remains nearly unchanged over 10,000 years, consistent with a quasi-steady reactive transport regime in which advective supply of Ra by upstream fluids is balanced by its removal through solid solution formation within the region.

3.4. Sensitivity analysis (SA) results

In the coprecipitation models, parameter variations primarily affect the amount and persistence of solid solution formation, while the overall spatiotemporal distribution patterns remain largely unchanged. Increased sulfate availability enhances early (Ba,Ra)SO_4 precipitation in fractures, followed by sulfate depletion and dissolution at later times (SA-1, Fig. 9). Elevated Ba^{2+} concentrations and higher Ba/Ra ratios in the inflowing fluid increase both the extent and persistence of coprecipitation relative to the baseline model (SA-2, Fig. 9). Higher flow velocities accelerate advective mixing between inflowing and resident fluids, leading to earlier precipitation and subsequent dissolution in fractures, with minimal impact on precipitation-dissolution patterns in the matrix (SA-3, Fig. 9). Variations in reactive surface area over one order of magnitude produce only minor effects on the resulting patterns (SA-4, Fig. 9; SA-5, Fig. 10). Increased diffusivity enhances early coprecipitation but accelerates late-stage dissolution and Ra remobilization by promoting Ra^{2+} diffusion into the matrix and more rapid sulfate depletion (SA-6, Fig. 10). Increasing dissolution rate constants sustains downstream supersaturation through enhanced upstream dissolution, thereby enhancing downstream coprecipitation (SA-7,

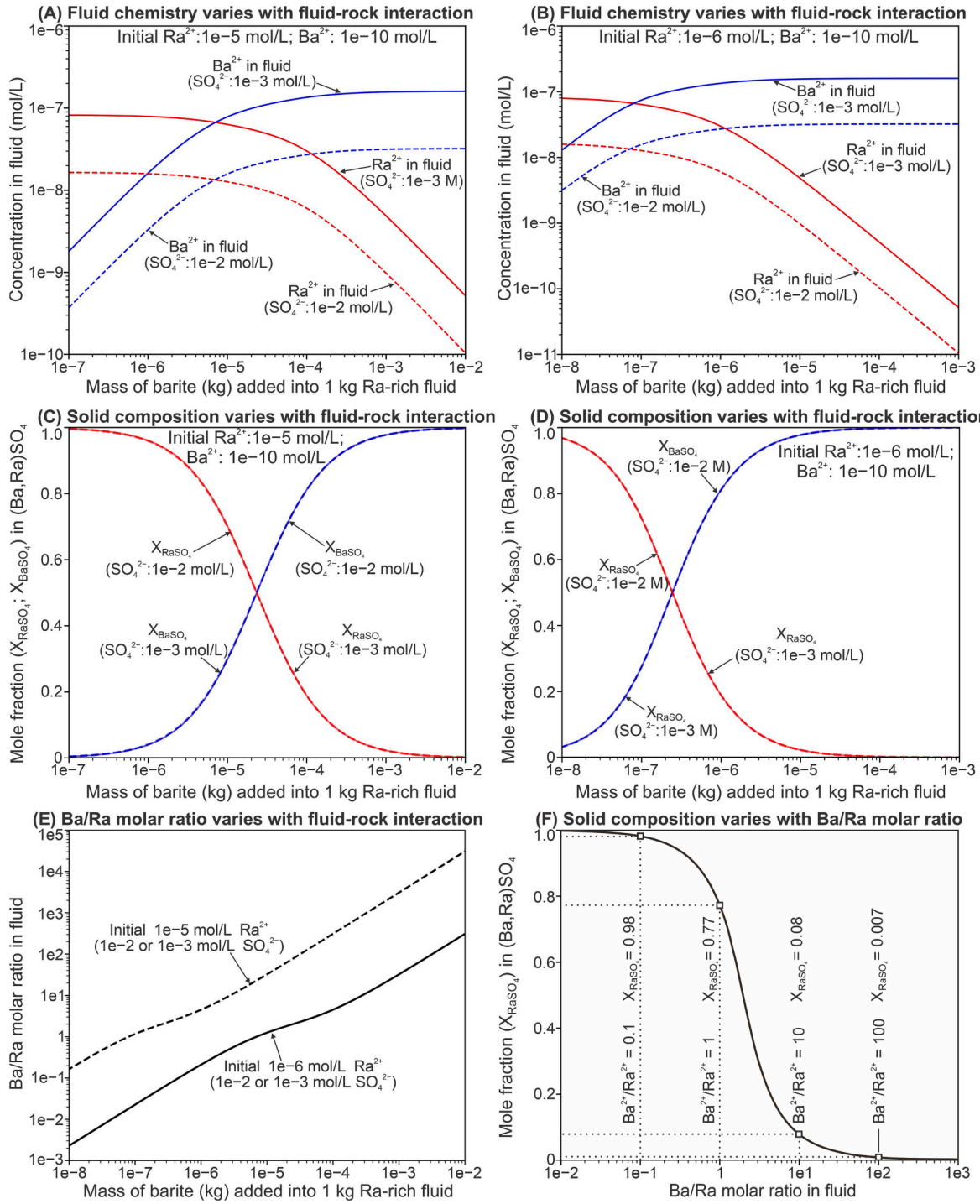

Fig. 4. Reaction path modeling results in which barite is incrementally added to 1 kg of Ra-rich fluids. (A) Ba^{2+} and Ra^{2+} concentrations as a function of the mass (kg) of barite added to a fluid initially containing 1×10^{-5} mol/L Ra^{2+}. (B) Same as (A), but for fluid initially containing 1×10^{-6} mol/L Ra^{2+}. (C) Composition of the precipitated solid solution, expressed as mole fractions X_{BaSO_4} and X_{RaSO_4}, during barite addition to a fluid with 1×10^{-5} mol/L Ra^{2+}. (D) Same as (C), but for fluid initially containing 1×10^{-6} mol/L Ra^{2+}. (E) Evolution of the Ba/Ra molar ratio during barite addition for different initial Ra^{2+} concentrations. (F) Modeled relationship between the Ba/Ra molar ratio and solid solution composition (X_{RaSO_4}), illustrating the shift toward $BaSO_4$-rich phases with increasing Ba/Ra ratios.

Fig. 10). Reducing the inflowing Ra concentrations to 1×10^{-9} mol/L substantially inhibits coprecipitation and favors the formation of Ba-dominated phases containing only trace amounts of Ra (SA-8, Fig. 10).

The recrystallization models show stronger sensitivity to parameters that control the spatial distribution and geometry of reaction fronts, where coupled barite dissolution and $(Ba,Ra)SO_4$ reprecipitation occur. Higher Ba^{2+} concentrations increase the amount and persistence of Ba-rich solid solutions (SA-9, Fig. 11). Higher flow rates promote more pervasive precipitation along fractures (SA-10, Fig. 11), whereas reduced initial barite availability leads to early precipitation within fractures, followed by dissolution and a transition toward matrix retention near fracture-matrix interfaces (SA-11, Fig. 11). Reactive surface area has a strong control on recrystallization patterns. Increasing surface area confines precipitation to narrow zones near fluid inlets (SA-12, Fig. 11), whereas decreasing surface area generates elongated, finger-shaped precipitation fronts extending farther downstream (SA-

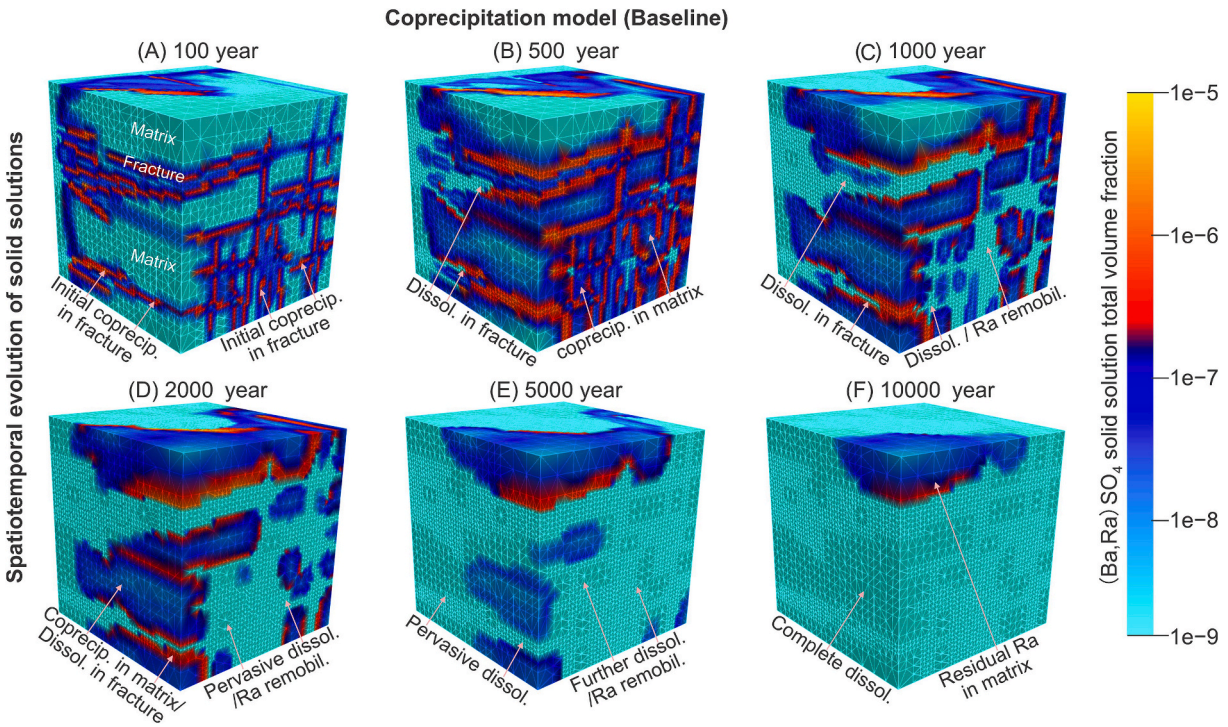

Fig. 5. Reactive transport modeling results for the baseline coprecipitation scenario, showing the spatiotemporal distribution of (Ba,Ra)SO_4 solid solutions within the modeled domain after (A) 100 years, (B) 500 years, (C) 1000 years, (D) 2000 years, (E) 5000 years, and (F) 10,000 years.

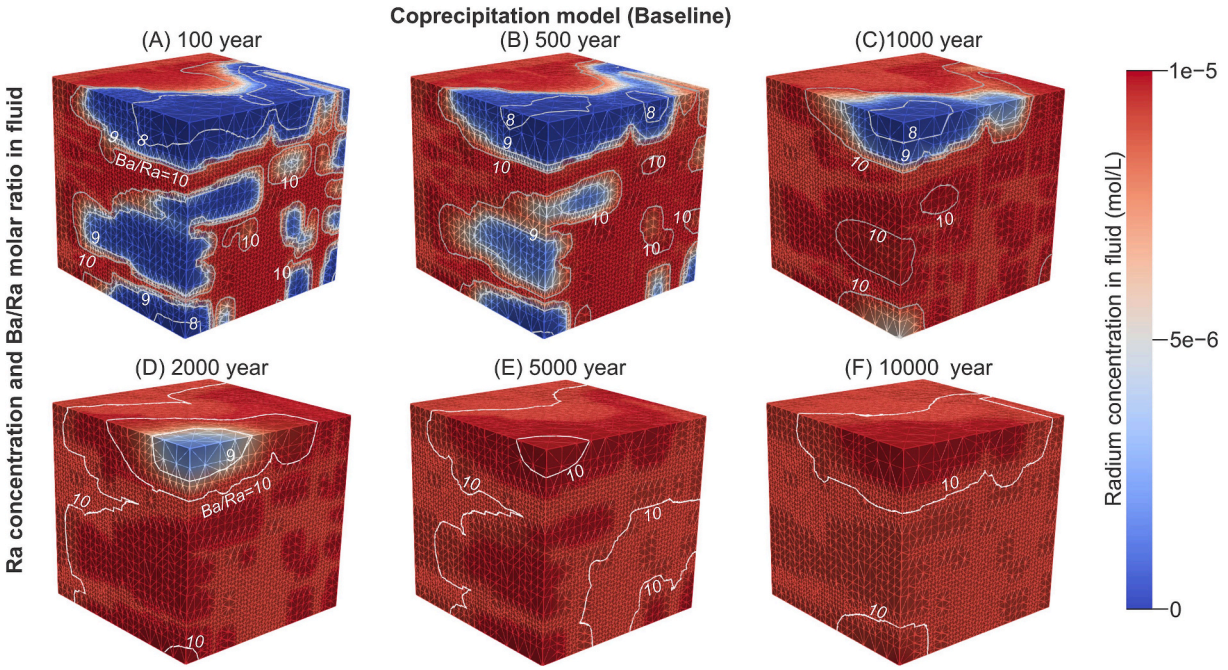

Fig. 6. Reactive transport modeling results for the baseline coprecipitation scenario, showing spatial distributions of Ra concentrations and Ba/Ra molar ratios within the modeled domain after (A) 100 years, (B) 500 years, (C) 1000 years, (D) 2000 years, (E) 5000 years, and (F) 10,000 years.

13, Fig. 12). Increased diffusivity broadens reaction fronts by enhancing transverse diffusion and penetration into the matrix (SA-14, Fig. 12). Increasing dissolution rate constant produces effects similar to increasing reactive surface area, promoting more localized recrystallization windows near the inlets and shortening reaction front lengths in fractures (SA-15, Fig. 12). Reducing the inflowing Ra concentration to 1×10^{-9} mol/L markedly limits both the spatial extent and temporal persistence of recrystallization (SA-16, Fig. 12).

Retention efficiencies show contrasting temporal trends between coprecipitation and recrystallization scenarios (Fig. 13C–D). In coprecipitation scenarios, retention generally declines rapidly with time, falling below 0.1 within ~1000 years. Elevated sulfate concentrations enhance retention (SA-1), whereas higher Ba^{2+} concentrations (SA-2), increased flow rates (SA-3), reduced mineral surface area (SA-5), increased dissolution rate constants (SA-7), and strongly reduced inflowing Ra^{2+} concentrations (SA-8) decrease retention efficiency.

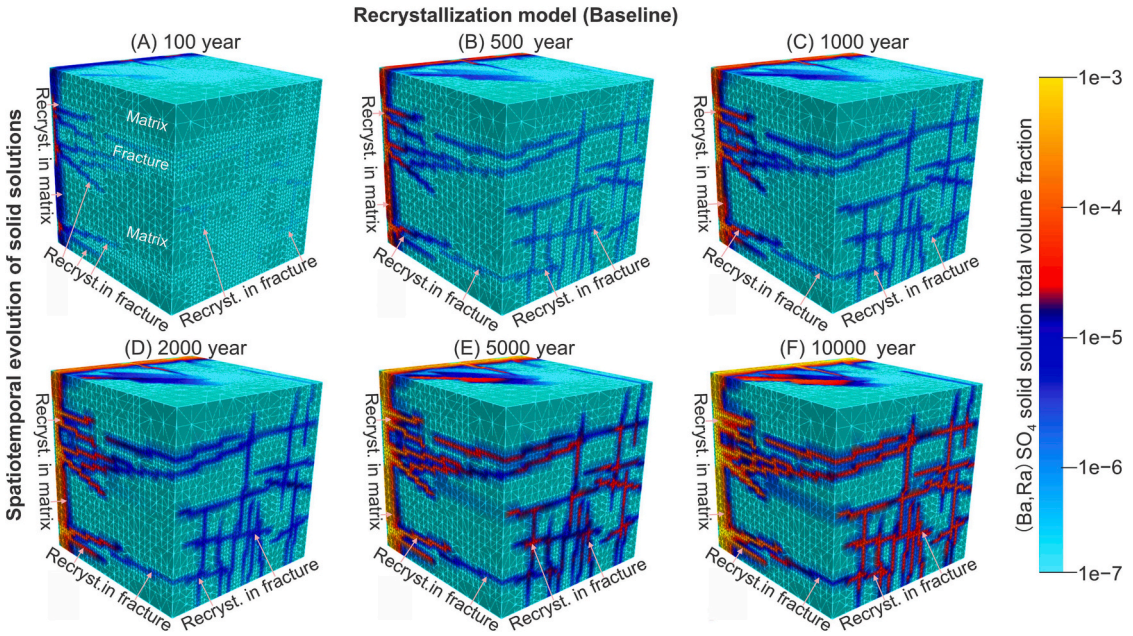

Fig. 7. Reactive transport modeling results for the baseline recrystallization scenario, showing the spatiotemporal distribution of $(Ba,Ra)SO_4$ solid solutions within the modeled domain after (A) 100 years, (B) 500 years, (C) 1000 years, (D) 2000 years, (E) 5000 years, and (F) 10,000 years.

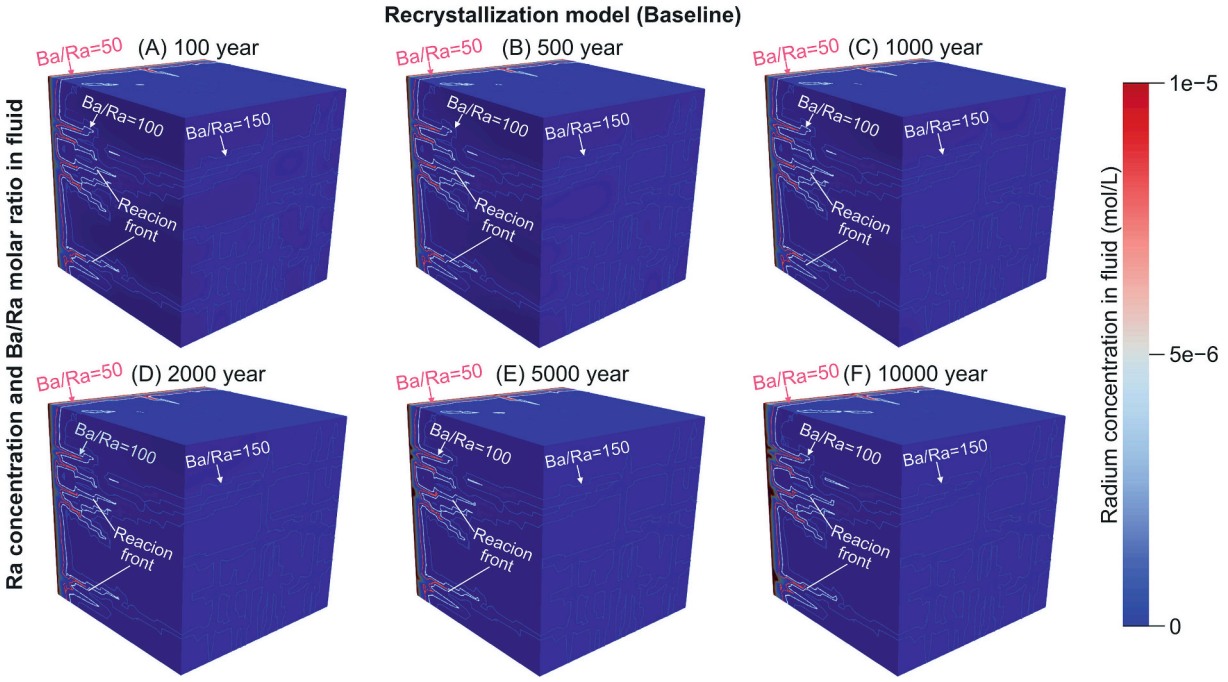

Fig. 8. Reactive transport modeling results for the baseline recrystallization scenario, showing spatial distributions of Ra concentrations and Ba/Ra molar ratios within the modeled domain after (A) 100 years, (B) 500 years, (C) 1000 years, (D) 2000 years, (E) 5000 years, and (F) 10,000 years.

Increasing specific surface area has little effect (SA-4), while higher diffusivity produces only a transient enhancement in retention before accelerating Ra remobilization compared to the baseline model (SA-6).

In contrast, recrystallization scenarios maintain consistently high retention efficiencies, generally exceeding 0.95 throughout the simulations. Higher Ba^{2+} concentrations (SA-9), increased flow rates (SA-10), and reduced reactive surface area (SA-13) result in only minor decreases in retention, whereas limited initial barite availability (SA-11) and very low inflowing Ra concentrations (SA-16) produce the largest declines. Increased reactive surface area (SA-12) and enhanced dissolution rate constants (SA-15) promote retention, while higher diffusivity (SA-14) initially reduces retention by enhancing early Ra transport out of the domain but increases long-term retention by promoting fracture-matrix exchange. Overall, under identical boundary conditions, recrystallization scenarios consistently yields substantially higher long-term Ra retention efficiency than coprecipitation scenarios (Fig. 13C–D).

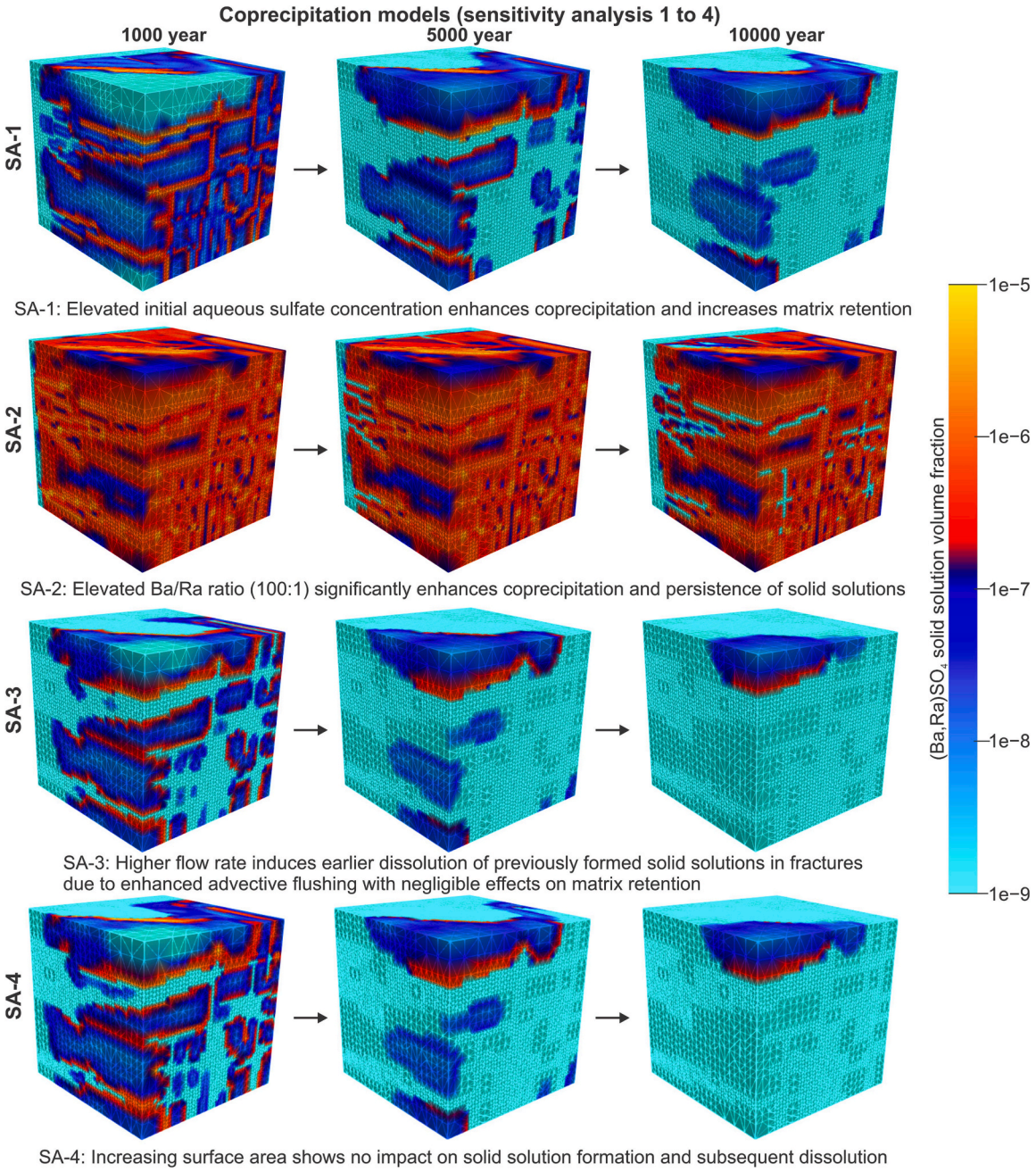

Fig. 9. Spatiotemporal evolution of solid solution distributions in coprecipitation models for sensitivity analyses SA-1 to SA-4 over 1000–10,000 years (see Table 2 for model setup details).

4. Discussion

4.1. Distinct mechanisms controlling Ra immobilization in fractured crystalline rocks

Although the microscopic geochemical mechanisms of Ra immobilization via coprecipitation and recrystallization have been extensively studied by experimental studies (Bosbach et al., 2010; Curti et al., 2010; Brandt et al., 2015; Poonoosamy et al., 2024), their effectiveness and spatiotemporal evolution at the field scale in fracture-matrix systems under reactive transport conditions remain poorly constrained. Our results show that, in barite-free zones, Ra retention is controlled by coprecipitation, which can be effective at early stages but is intrinsically transient because it depends on aqueous sulfate availability, which controls the persistence of mixing-induced supersaturation. In contrast, in barite-bearing zones, Ra immobilization is dominated by kinetically controlled recrystallization, enabling sustained Ra retention through coupled barite dissolution and (Ba,Ra)SO_4 solid solution reprecipitation over geological timescales.

In fractures, recrystallization generates reaction fronts characterized by pronounced compositional zonation, with Ra-rich solid solutions forming near fluid inlets and progressively Ba-richer compositions developing downstream (Fig. 7). These patterns reflect transport-controlled reaction disequilibrium, which can be quantified using Damköhler numbers (Da $<$ 1; e.g., Seigneur et al., 2019), indicating that advective Ra transport overwhelms the kinetics of Ra incorporation into barite through recrystallization. As a result, the advective Ra flux exceeds the local capacity of recrystallization to immobilize Ra near inflow regions, producing elongated reaction fronts extending along fracture networks (Fig. 7). Increasing Damköhler numbers, through reduced flow

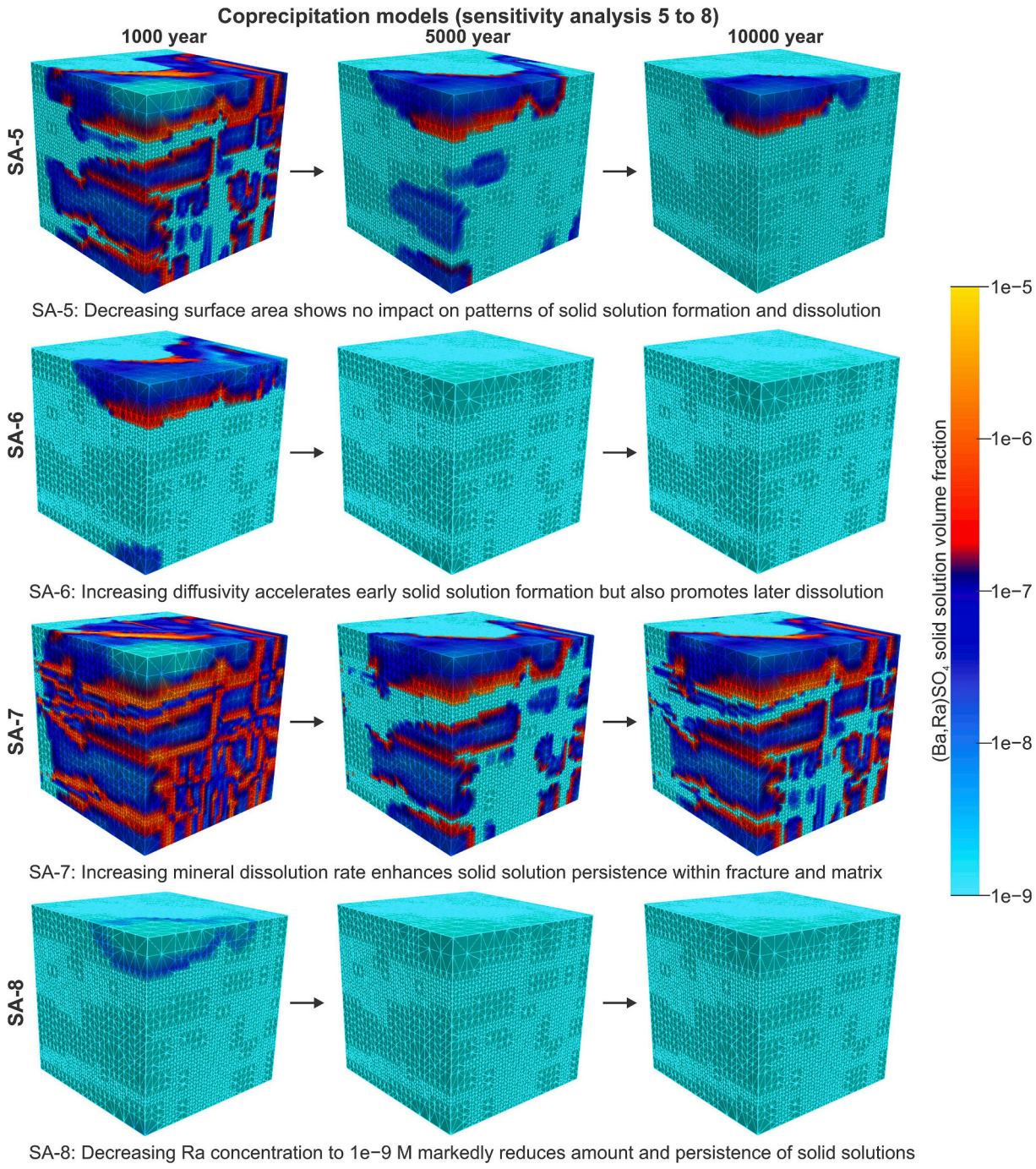

Fig. 10. Spatiotemporal evolution of solid solution distributions in coprecipitation models for sensitivity analyses SA-5 to SA-8 over 1000–10,000 years (see Table 2 for model setup details).

velocities, increased mineral surface areas, or elevated dissolution rate constants, enhances the relative importance of reaction kinetics over advective transport, promotes the development of near-equilibrium conditions close to fluid inlets, and thereby confines Ra uptake to narrower zones, limits downstream migration, and increases overall retention efficiency.

In contrast, coprecipitation in fractures does not develop comparable reaction front structures because it is driven by highly supersaturated conditions generated by fluid mixing, which are inherently transient when sulfate is displaced by sustained flushing (Fig. 6). Unlike recrystallization, coprecipitation does not involve a rate-limiting barite dissolution step and is therefore only weakly sensitive to mineral dissolution kinetics. During early-stage mixing, high supersaturation leads to high Damköhler numbers, allowing precipitation to proceed rapidly relative to advective transport and to approach local equilibrium in fracture zones. However, continued flushing progressively depletes sulfate and collapses supersaturation, causing coprecipitation to cease. As undersaturation develops in fractures, previously formed solid solutions dissolve and Ra is remobilized and flushed from the domain. Consequently, the spatiotemporal extent of coprecipitation is primarily controlled by transient sulfate availability, such that the inherent instability of sulfate distributions results in transient Ra retention in fractures (Fig. 5).

Transport within the rock matrix is diffusion-dominated, and therefore solute residence times are sufficiently long for local equilibrium conditions (Da $>$ 1) to be attained, enabling efficient Ra immobilization

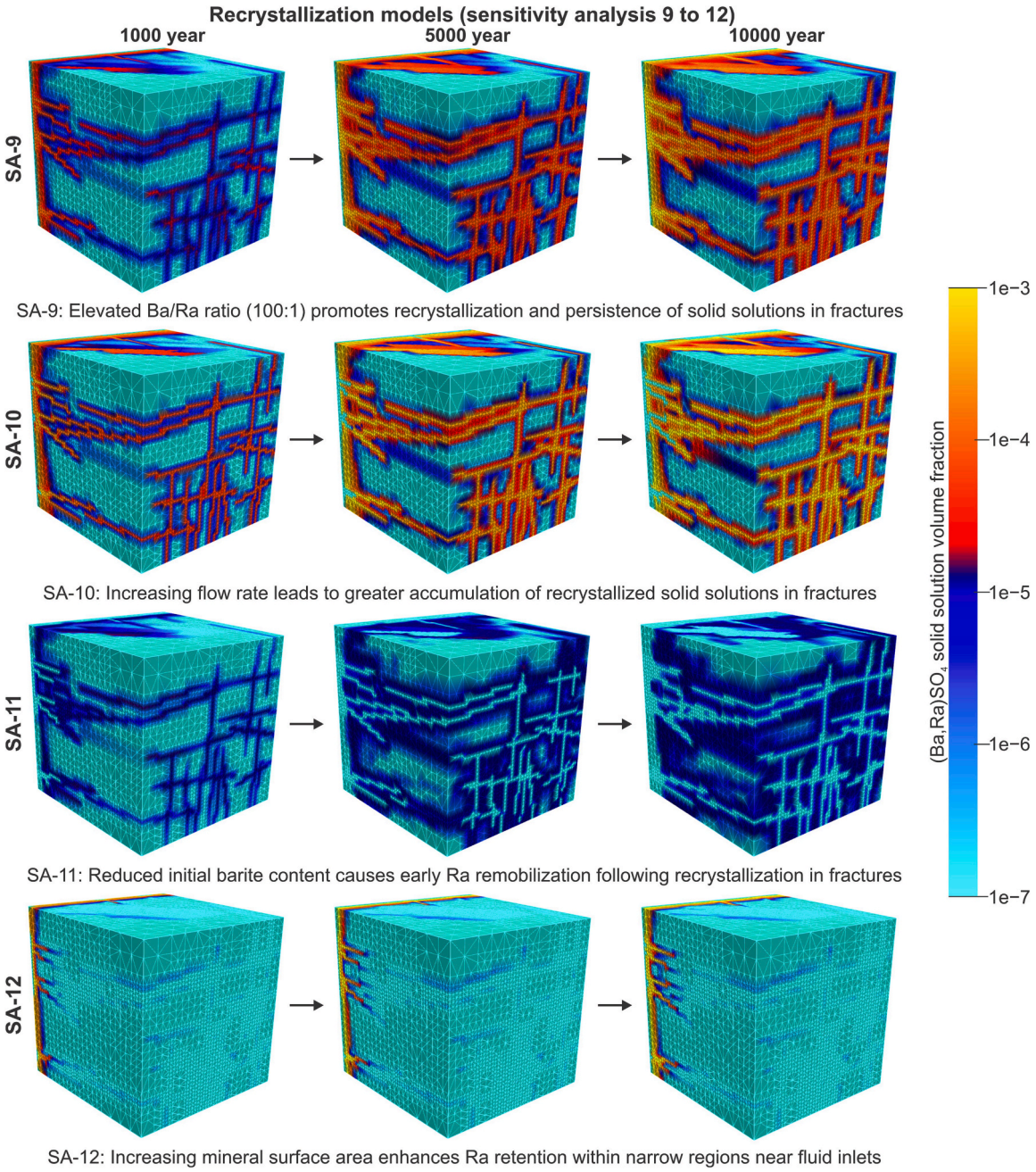

Fig. 11. Spatiotemporal evolution of solid solution distributions in recrystallization models for sensitivity analyses SA-9 to SA-12 over 1000–10,000 years (see Table 2 for model setup details).

within matrix domains by either coprecipitation or recrystallization. Barite abundance has a critical control on the persistence of recrystallization. When barite content in fractures is limited (e.g., 0.01%), recrystallization-controlled immobilization is initially effective but becomes transient once reactive barite is exhausted, causing Ra retention to progressively shift toward diffusion-dominated matrix zones (SA-11, Fig. 11). This represents a transitional case between recrystallization-dominated and coprecipitation-dominated systems, in which the overall retention efficiency is initially high but declines rapidly following barite depletion, ultimately approaching the low values characteristic of transient coprecipitation scenarios at long timescales (SA-11, Fig. 13D).

Thermodynamic reaction path modeling predicts enhanced Ra immobilization at high Ba/Ra ratios through the “dilution effect”, such that aqueous Ra concentrations become extremely low when the fluid is in equilibrium with Ba-dominated phases (Fig. 4A–B). This interpretation has led to the expectation that increasing Ba/Ra ratios alone could reduce aqueous Ra concentrations and thereby limit Ra migration in groundwater systems (e.g., Grandia et al., 2008; Vinograd et al., 2013). However, our modeling results show that under reactive transport conditions, elevated Ba/Ra ratios consistently reduce Ra retention efficiency in both coprecipitation and recrystallization scenarios (Fig. 13C–D), but for different mechanistic reasons. In coprecipitation scenarios, high Ba/Ra ratios favor rapid precipitation of Ba-rich phases that efficiently consume sulfate but incorporate little Ra, leaving a substantial fraction of Ra in the aqueous phase that is rapidly advected out of the system. In recrystallization scenarios, elevated Ba/Ra ratios inhibit barite dissolution, the rate-limiting step for subsequent (Ba,Ra)SO_4 reprecipitation, and thus limit subsequent Ra incorporation into solid phases. These results demonstrate that equilibrium-based predictions cannot be directly extrapolated to open, flow-through reactive

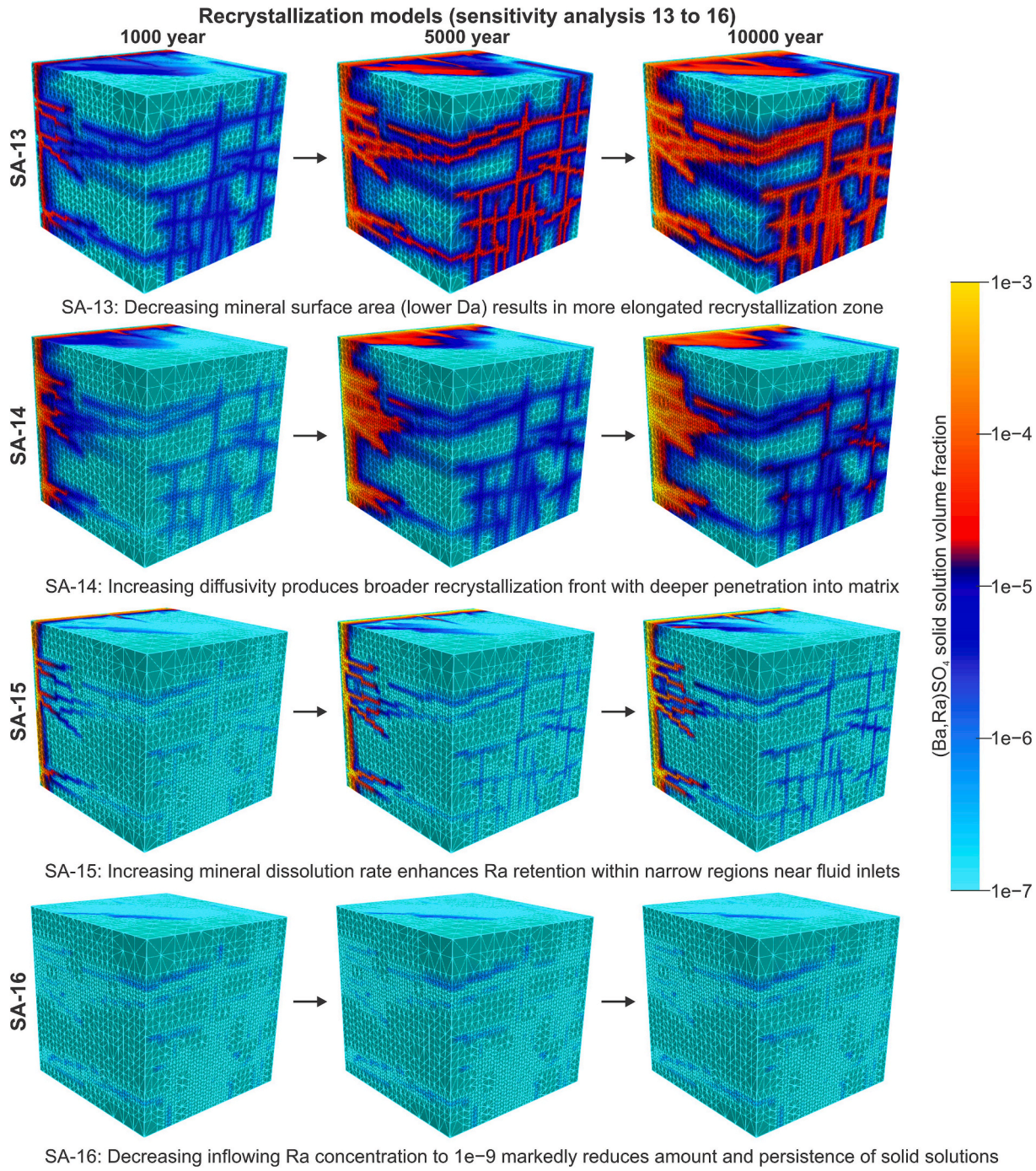

Fig. 12. Spatiotemporal evolution of solid solution distributions in recrystallization models for sensitivity analyses SA-13 to SA-16 over 1000–10,000 years (see Table 2 for model setup details).

transport environments, in which non-equilibrium geochemical reactions interact with flow and transport to control Ra mobility.

A further key finding is that to sustain high Ra immobilization efficiency (e.g., >0.8) requires fractures to act as the dominant retention domains, irrespective of whether coprecipitation or recrystallization dominates. This contrasts with conventional models that emphasize matrix storage and retention (e.g., sorption) while regarding fractures primarily as transport pathways (Zuber and Motyka, 1994; Roubinet et al., 2012; Zhang et al., 2022; Yang et al., 2024). In crystalline rocks, where matrix porosity is typically <2% and permeability is several orders of magnitude lower than that of fractures, fracture-matrix mass exchange is minimal compared to advective transport in fractures (Tsang et al., 2015; Steefel and Hu, 2022). Consequently, Ra that is not immobilized within fracture zones, is rapidly flushed from the system before significant uptake in the rock matrix can occur. Enhancing the retention capacity of fracture networks, rather than relying on diffusive matrix storage, therefore emerges as the most effective strategy for achieving long-term immobilization of Ra and other radionuclides in fractured crystalline rocks.

4.2. Comparison with previous experiments

Experimental studies show that coprecipitation proceeds rapidly because supersaturation develops immediately upon mixing Ba/Ra-

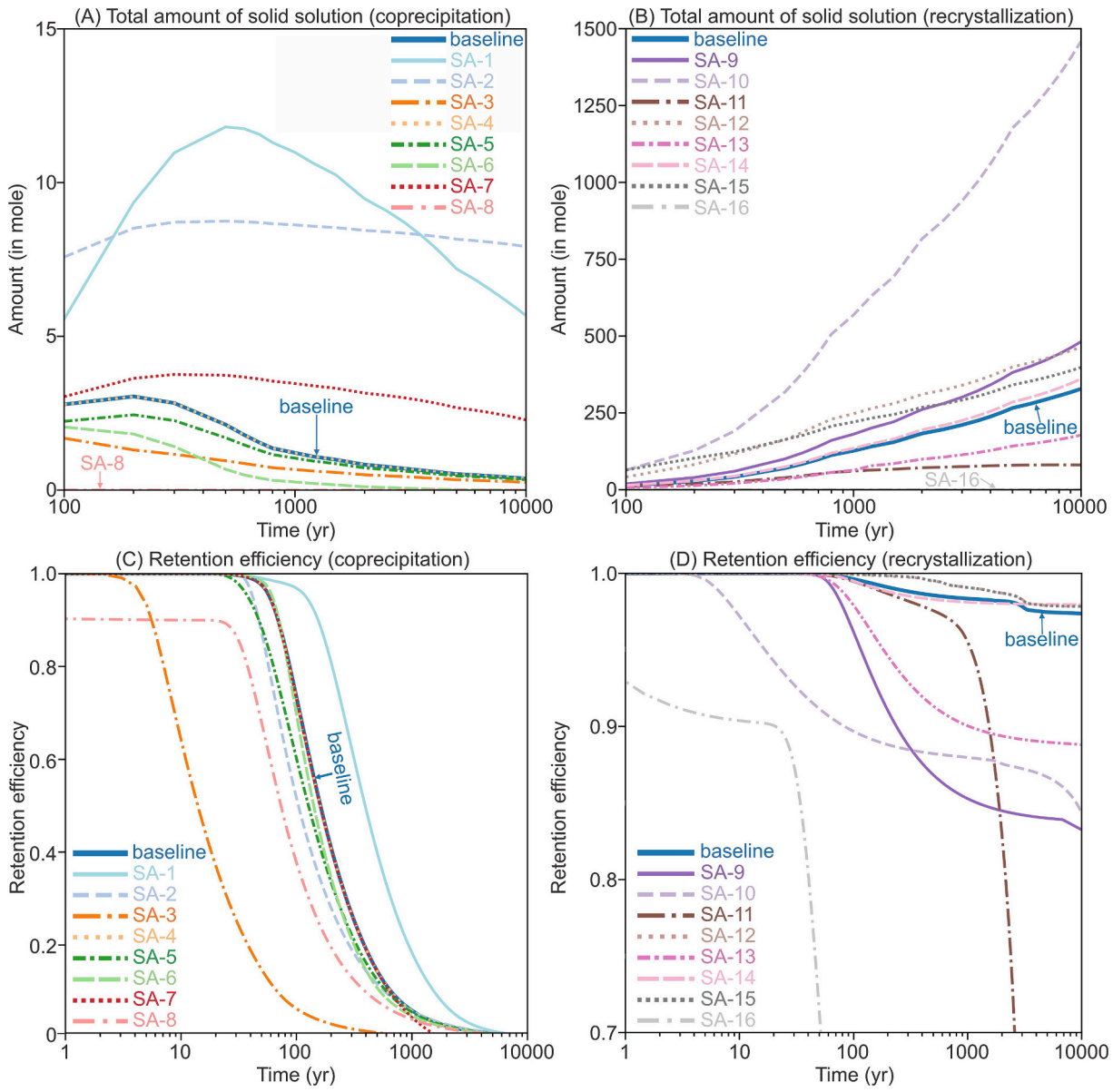

Fig. 13. Total amount of $(Ba,Ra)SO_4$ formed in coprecipitation (A) and recrystallization (B) scenarios. Ra retention efficiency in coprecipitation (C) and recrystallization (D) scenarios.

bearing and sulfate-rich fluids, enabling fast nucleation and growth of $(Ba,Ra)SO_4$ solid solutions (Doerner and Hoskins, 1925; Rosenberg et al., 2014, 2018; Poonoosamy et al., 2024). Microfluidic experiments further demonstrate that $Ba_{0.5}Ra_{0.5}SO_4$ can precipitate within hours from highly supersaturated solutions resulting from fluid mixing (Poonoosamy et al., 2024). These timescales are orders of magnitude shorter than those considered in our reactive transport models. Consequently, while coprecipitation is fundamentally a kinetic process, it effectively attains local equilibrium on timescales relevant to field-scale modeling. Our results further indicate that kinetic limitations become significant only at extremely low specific surface areas (e.g., 0.1 m^{-1}), where reduced precipitation and dissolution rates shift the system from reaction-dominated to transport-dominated (SA-5, Fig. 10). Under these conditions, coprecipitation timescales become comparable to transport timescales, preventing rapid equilibrium and allowing multiple metastable phases to coexist. These results suggest that, under most geological conditions, coprecipitation can be reasonably approximated as a local equilibrium process, despite being kinetically controlled at shorter timescales in laboratory experiments.

In contrast, recrystallization proceeds much more slowly than coprecipitation because it requires barite dissolution before $(Ba,Ra)SO_4$ reprecipitation, rendering barite dissolution the rate-limiting step. Even though $(Ba,Ra)SO_4$ precipitation is kinetically fast, the slow release of sulfate during barite dissolution limits the overall rate of Ra uptake (Ruiz-Agudo et al., 2014; Konrad-Schmolke et al., 2018). Experimental observations clearly show that recrystallization requires substantially longer timescales. Radiotracer experiments using ^{133}Ba and ^{226}Ra, combined with fluid composition analyses (ICP-MS, ion chromatography) and solid-phase characterization (SEM, BET), show that Ra uptake may require more than three years to approach equilibrium (Bosbach et al., 2010; Curti et al., 2010). Furthermore, barite preequilibrated with aqueous solutions shows markedly reduced reactivity, with only ~7% recrystallization occurring after five years (Heberling et al., 2018). The decrease in reactivity is attributed to Ostwald ripening, which progressively reduces reactive surface area, limiting barite dissolution and Ra incorporation (Steefel and Van Cappellen, 1990).

Our modeling results capture these experimental kinetic constraints

by representing barite dissolution as the rate-limiting step of a coupled dissolution-reprecipitation process. Under high barite supersaturation ratios, resulting from elevated Ba concentrations (SA-9, Fig. 11) or decreased reactive surface area (SA-13, Fig. 12), Ra uptake through recrystallization proceeds slowly, producing elongated reaction fronts. In contrast, increasing reactive surface area (SA-12, Fig. 11) or dissolution rate constants (SA-15, Fig. 12) enhances barite dissolution, increases Ra uptake rates, and results in narrower reaction fronts. Together, experimental and modeling results demonstrate that recrystallization remains kinetically controlled across laboratory, modeling, and natural geological timescales, and cannot be approximated as a local equilibrium process in reactive transport models.

In our models, newly formed solid solutions are assumed to be compositionally homogeneous, without resolving microscopic zonation or compositional heterogeneity within individual crystals (Putnis, 2009; Ruiz-Agudo et al., 2014). This simplification reflects an inherent limitation of the continuum-scale reactive transport modeling (Molins and Knabner, 2019; Zhang et al., 2026). At the nanoscale, transient nanoscale compositional and structural heterogeneities have been documented using high-resolution electron microscopy and atomic probe tomography (Weber et al., 2016,2017). Similarly, pore-size-dependent solubility effects may locally affect aqueous Ra concentrations in nanopores (Liu and Jacques, 2017; Poonoosamy et al., 2023). However, these effects are most pronounced at nanometer- to micrometer-scales and are therefore likely to be averaged out at the field scale investigated in this study. While such microscale processes may introduce local deviations from model predictions, they are unlikely to change the dominant controlling factors or overall patterns of Ra immobilization identified here. Upscaling these microscale effects to field-scale models lies beyond the scope of the present study but warrants further investigation.

4.3. Implications for natural and engineered systems

Hydrothermal barite veins preserved in fractures over millions of years provide compelling geological evidence for the long-term geochemical stability of barite under fracture-controlled reactive flow conditions (Dill, 1988; Wind et al., 2023). These natural analogues demonstrate that fractures act not only as preferential pathways for fluid flow and mass transport, but also as persistent reactive domains capable of immobilizing Ra over geological timescales. Although natural barite typically contains only trace amounts of Ra, elevated radioactivity of ~10 Bq/g (corresponding to ~0.3 ng/g Ra) has been reported in barite from natural mineral deposits (Ulrych et al., 2007; Jirásek et al., 2020). These values are substantially lower than those observed in anthropogenic barite formed in U mining tailings or oilfield scales, where radioactivity commonly exceeds 1000 Bq/g (IAEA, 2003). Nevertheless, such natural enrichments are noteworthy given the relatively short half-life of ^{226}Ra (~1600 years) and the potential loss of Ra decay products (e.g., ^{222}Rn) from mineral lattices over time. For example, Ra-rich barite with an initial activity of 100 Bq/g would decay to ~1.3 Bq/g after 10,000 years in the absence of Ra replenishment. The occurrence and persistence of Ra-enriched hydrothermal barite therefore likely reflect either relatively recent fluid-rock interaction involving coprecipitation during fluid mixing, or repeated episodes of barite recrystallization that continuously incorporate Ra. Because Ra is a major decay product of U, such enrichments may indicate hydrothermal reworking of U deposits, Ra mobilization along structurally reactivated faults (Wang and Chi, 2023), or circulation of metal-bearing hydrothermal fluids (Wang et al., 2021,2025). Given its higher mobility than U and weaker sensitivity to sorption and redox conditions, Ra-rich barite may thus serve as a sensitive geochemical indicator for U mineralization, consistent with field observations near U deposits, where barite records repeated cycles of dissolution and reprecipitation that incorporate Ra released from U ores into mineral lattices (Denton et al., 2016).

Coprecipitation is kinetically fast but provides only transient immobilization, making it well suited for short-term mitigation of Ra release, such as during early leakage events or rapid pollution plume migration, where the targeted addition of Ba^{2+} and sulfate can induce immediate immobilization (Grandia et al., 2008; Curti et al., 2019; Poonoosamy et al., 2024). However, because its effectiveness depends on sustained sulfate availability, coprecipitation is unlikely to persist under repository conditions where groundwater flow regimes and chemistry evolve and sulfate may become depleted over time. In contrast, recrystallization is kinetically slower but capable of sustaining Ra immobilization in the near-field conditions over geological timescales (e.g., >10,000 years), particularly in barite-bearing fracture-matrix systems of crystalline rocks (Bosbach et al., 2010; Curti et al., 2010; Brandt et al., 2015). These contrasting behaviors indicate that coprecipitation is best suited for short-term engineering interventions in dynamic hydrological settings, such as enhanced geothermal systems or shale gas reservoirs, whereas recrystallization provides the long-term retention capacity critical for repository performance. Accordingly, the establishment of barite-bearing buffer layers should be considered during repository design or pre-closure conditioning to enhance long-term Ra retention.

In real-world repository systems, Ra release from corroded waste canisters to fractured crystalline rocks is controlled by several coupled factors. These include: (1) the timing and mode of canister failure, which control the onset and rate of Ra release through spent fuel degradation and corrosion products into groundwater (SKB, 2011); (2) fluid-waste interactions involving dissolution-precipitation reactions, redox processes, secondary phase formation, and metal leaching (Tsang et al., 2015); (3) multicomponent aqueous chemistry, in which competing divalent cations (e.g., Ba^{2+}, Sr^{2+}) affect Ra solubility and mobility (Klinkenberg et al., 2018; Vinograd et al., 2018); and (4) engineered buffer materials (e.g., bentonite), which further modify pore water composition and near-field transport conditions (Ait-Mouheb et al., 2024). As a result, a wide range of plausible Ra source concentrations may enter fractured crystalline rocks. For example, safety assessment studies by Nagra typically consider Ra concentrations of $\leq 10^{-8}$ mol/L (Nagra, 2002), whereas higher concentrations of $\sim 10^{-5}$ mol/L are considered for cemented intermediate-level waste (Gaucher and Blanc, 2006). Accordingly, high (10^{-5} mol/L) and low (10^{-9} mol/L) Ra source terms were evaluated as bounding cases representing different release scenarios. Modeling results show that, although the Ra source term affects the spatial extent and temporal persistence of Ra immobilization, it does not alter the spatiotemporal patterns of $(Ba,Ra)SO_4$ solid solution formation or the contrasting retention efficiencies associated with coprecipitation and recrystallization mechanisms.

Overall, this study demonstrates that mechanistic differences at the microscopic scale can lead to contrasting field-scale behaviors when coupled with flow and transport in heterogeneous geological media. Although coprecipitation and recrystallization both form $(Ba,Ra)SO_4$ solid solutions, they generate distinct spatiotemporal patterns of Ra retention. Several geochemical processes not considered here, such as microbial sulfate reduction (Phillips et al., 2001; Drake et al., 2017) and competitive incorporation of Sr in ternary $(Ba,Sr,Ra)SO_4$ solid solutions (Klinkenberg et al., 2018; Vinograd et al., 2018), may further affect Ra immobilization. In addition, the solid solution-aqueous solution model adopted here is based on a stoichiometric saturation model that approximates, but does not fully represent, true thermodynamic equilibrium (Prieto, 2009). While these factors introduce additional complexity and may lead to deviations from the results presented here, they are not expected to alter the contrasting mechanisms of coprecipitation and recrystallization, nor the roles of fractures and the matrix in controlling Ra immobilization identified in this study. Accurate prediction of absolute Ra concentrations and solid solution compositions over long-term evolution in geological repository systems therefore remains a challenging task for reactive transport modeling. Despite these limitations, our results highlight that effective Ra immobilization in fractured crystalline rocks depends on the coupled spatiotemporal evolution of

fracture-matrix hydrogeology, reaction mechanisms and kinetics, and hydrogeochemical conditions. Integrating these coupled processes within 3D reactive transport models provides a robust framework for evaluating long-term radionuclide behavior at repository sites, testing contamination scenarios, and supporting scenario-based safety assessments (Lichtner and Carey, 2006; Marty et al., 2009; Steefel et al., 2015; Hyman et al., 2024).

5. Conclusions

This study demonstrates that Ra immobilization via (Ba,Ra)SO_4 solid solution formation in fractured crystalline rocks is controlled by contrasting coprecipitation and recrystallization mechanisms. Coprecipitation proceeds rapidly under mixing-induced supersaturation but provides only transient immobilization, as sustained groundwater flushing progressively depletes sulfate and promotes dissolution of previously formed solid solutions and Ra remobilization. In contrast, recrystallization is a kinetically controlled coupled dissolution–recrystallization process, in which barite dissolution acts as the rate-limiting step, yet it enables sustained Ra immobilization over geological timescales. Differences in microscopic differences between coprecipitation and recrystallization are strongly expressed at the field scale through their coupling with heterogeneous flow and transport in fracture-matrix systems, leading to distinct spatiotemporal distributions of (Ba,Ra)SO_4 solid solutions and systematically different trends in retention efficiency. Across all modeling scenarios, sustained high retention efficiency is achieved only when fractures act as the dominant reactive domains for Ra immobilization, whereas the low-permeability rock matrix contributes minimally due to limited diffusive exchange. Consequently, Ra that is not retained within fracture zones is preferentially flushed from the domain rather than being retained within matrix domains. Furthermore, our results suggest that equilibrium-based predictions, including the commonly invoked “dilution effect”, cannot be directly extrapolated to open, flow-through hydrogeochemical systems. Robust assessment of Ra mobility in fractured crystalline rocks therefore requires coupling of reaction mechanisms and kinetics with flow and transport processes in evolving fracture-matrix systems. Overall, these findings provide new mechanistic insights into Ra mobility in groundwater systems, with implications for nuclear waste disposal safety, contaminant management, geothermal resource exploitation, and the long-term mobility of trace elements in complex subsurface environments.

Data availability

Data are available through Mendeley Data at https://doi.org/10.17632/cnrvgjzwdc.2.

CRediT authorship contribution statement

Yumeng Wang: Writing – review & editing, Writing – original draft, Visualization, Validation, Software, Resources, Project administration, Methodology, Investigation, Formal analysis, Data curation, Conceptualization. **Peter Alt-Epping:** Writing – review & editing, Visualization, Validation, Software, Resources, Methodology, Formal analysis, Data curation. **Guido Deissmann:** Writing – review & editing, Validation, Resources, Methodology, Formal analysis, Data curation. **Yuankai Yang:** Writing – review & editing, Validation, Methodology, Data curation. **Jun Hu:** Writing – review & editing, Validation, Data curation. **Dirk Bosbach:** Writing – review & editing, Validation, Resources, Formal analysis, Data curation. **Jenna Poonoosamy:** Writing – review & editing, Visualization, Validation, Resources, Project administration, Methodology, Funding acquisition, Formal analysis, Data curation.

Declaration of competing interest

The authors declare that they have no known competing financial interests or personal relationships that could have appeared to influence the work reported in this paper.

Acknowledgement

The research was primarily supported by the European Research Council through the GENIES project (ERC, grant agreement 101040341). The authors gratefully acknowledge the computing time on the JURECA supercomputer at the Jülich Supercomputing Center under the grant MAGIE. Y.W. thanks Dr. Glenn Hammond for helpful discussions on PFLOTRAN implementation and high-performance parallel computing for reactive transport modeling, and Dr. Victor Vinograd for valuable scientific insights into the thermodynamics of non-ideal solid solutions. The authors thanks Dr. Christophe Tournassat and Dr. Hailiang Dong for their editorial handling, and the constructive feedback and comments from two anonymous reviewers, which helped significantly improve the quality of this manuscript.

Appendix A. Supplementary material

The supplementary material (SM) provides additional thermodynamic, kinetic, and modeling results supporting this study. It includes stoichiometric solubility products (K_{st}) for ideal and non-ideal (Ba,Ra)SO_4 solid solutions calculated using Guggenheim interaction parameters (SM Table S1), precipitation rate constants for barite, $RaSO_4$, and (Ba,Ra)SO_4 solid solutions used in the reactive transport modeling (SM Table S2), and the stoichiometric solid solutions used in baseline models and sensitivity analyses (SM Table S3). The temporal evolution of the total amounts of discrete (Ba,Ra)SO_4 solid solutions in the baseline coprecipitation and recrystallization models and associated sensitivity analyses is shown in SM Fig. S1 and SM Fig. S2, respectively. Supplementary material to this article can be found online at https://doi.org/10.1016/j.gca.2026.01.045.

References

Ait-Mouheb, N., Yang, Y., Deissmann, G., Klinkenberg, M., Poonoosamy, J., Vinograd, V., Van Loon, L.R., Bosbach, D., 2024. Retention of ^{226}Ra in the sandy Opalinus Clay facies from the Mont Terri rock laboratory. Switzerland. Appl. Geochem. 170, 106048.

Andrews, E.M., Hyman, J.D., Sweeney, M.R., Karra, S., Moulton, J.D., Navarre-Sitchler, A., 2023. Fracture intensity impacts on reaction front propagation and mineral weathering in three-dimensional fractured media. Water Resour. Res. 59, e2022WR032121.

Berner, U., Curti, E., 2002. Radium solubilities from SF/HLW wastes using solid solution and co-precipitation models, Report TM-44-02-04. Paul Scherrer Institute, Villigen, Switzerland.

Besançon, C., Gérard, M., Lahrouch, F., Hughes, K., Sardini, P., Savoye, S., Descostes, M., 2025. Confirmation of the retention of ^{226}Ra in U mine tailings by barite. J. Hazard. Mater. Adv. 18, 100716.

Bethke, C.M., 2022. Geochemical and Biogeochemical Reaction Modeling, third ed. Cambridge University Press, Cambridge, UK, p. 502.

Bons, P.D., Elburg, M.A., Gomez-Rivas, E., 2012. A review of the formation of tectonic veins and their microstructures. J. Struct. Geol. 43, 33–62.

Bosbach, D., 2002. Linking molecular-scale barite precipitation mechanisms with macroscopic crystal growth rates. In: Hellmann, R., Wood, S.A. (Eds), Water-Rock Interactions, Ore deposits, and Environmental Geochemistry: A tribute to David A. Crerar, Geochemical Society Special Publication No. 7, pp. 97–110.

Bosbach, D., Böttle, M., Metz, V., 2010. Experimental study on Ra^{2+} uptake by barite ($BaSO_4$). SKB Technical Report TR-10-43. Stockholm, Sweden. p. 111.

Bosbach, D., Brandt, F., Bukaemskiy, A., Deissmann, G., Kegler, P., Klinkenberg, M., Kowalski, P.M., Modolo, G., Niemeyer, I., Neumeier, S., Vinograd, V., 2020. Research for the safe management of nuclear waste at Forschungszentrum Jülich: material chemistry and solid solution aspects. Adv. Eng. Mater. 22, 1901417.

Boumaiza, L., Stotler, R., Frape, S., 2024. A review of the major chemical and isotopic characteristics of groundwater in crystalline rocks of the Canadian Shield. Chem. Geol. 669, 122366.

Brandt, F., Curti, E., Klinkenberg, M., Rozov, K., Bosbach, D., 2015. Replacement of barite by a (Ba,Ra)SO_4 solid solution at close-to-equilibrium conditions: a combined experimental and theoretical study. Geochim. Cosmochim. Acta 155, 1–15.

Brandt, F., Klinkenberg, M., Poonoosamy, J., Bosbach, D., 2020. Recrystallization and uptake of ^{226}Ra into Ba-rich (Ba,Sr)SO_4 solid solutions. Minerals 2020 (10), 812.
Brace, W., 1984. Permeability of crystalline rocks: New in situ measurements. J. Geophys. Res. 89, 4327–4330.
Christy, A.G., Putnis, A., 1993. The kinetics of barite dissolution and precipitation in water and sodium chloride brines at 44–85°C. Geochim. Cosmochim. Acta 57, 2161–2168.
Coleman, T.I., Parker, B.L., Maldaner, C.H., Mondanos, M.J., 2015. Goundwater flow characterization in a fractured bedrock aquifer using active DTS tests in sealed boreholes. J. Hydrol. 528, 449–462.
Curti, E., Fujiwara, K., Iijima, K., Tits, J., Cuesta, C., Kitamura, A., Glaus, M.A., Müller, W., 2010. Radium uptake during barite recrystallization at 23 ± 2°C as a function of solution composition: an experimental ^{133}Ba and ^{226}Ra tracer study. Geochim. Cosmochim. Acta 74, 3553–3570.
Curti, E., Xto, J., Borca, C.N., Henzler, K., Huthwelker, T., Prasianakis, N.I., 2019. Modeling of Ra-bearing baryte nucleation/precipitation kinetics at the pore scale: application to radioactive waste disposal. Eur. J. Min. 31, 247–262.
Dideriksen, K., Christiansen, B.C., Frandsen, C., Balic-Zunic, T., Morup, S., Stipp, S.L.S., 2010. Paleo-redox boundaries in fractured granite. Geochim. Cosmochim. Acta 74, 2866–2880.
Dill, H., 1988. Geologic setting and age relationship of fluorite-barite mineralization in Southern Germany with special reference to the late Paleozoic unconformity. Min. Depos. 23, 16–23.
Denton, J.S., Goldstein, S.J., Paviet, P., Nunn, A.J., Amato, R.S., Hinrichs, K.A., 2016. A record of uranium-series transport at Nopal I, Sierra Peña Blanca, Mexico: Implications for natural uranium deposits and radioactive waste repositories. Chem. Geol. 434, 12–27.
Doerner, H.A., Hoskins, W.M., 1925. Co-precipitation of radium and barium sulphates. J. Am. Chem. Soc. 47, 662–675.
Doolaeghe, D., Darcel, C., Selroos, J.O., Mas Ivars, D., Davy, P., 2023. Controls on fracture openness and reactivation in Forsmark, Sweden. Sci. Rep. (2023)13, 6686.
Drake, H., Ivarsson, M., Bengtson, S., Heim, C., Silkeström, S., Whitehouse, M.J., Broman, C., Belivanova, V., Åström, M.E., 2017. Anaerobic consortia of fungi and sulfate reducing bacteria in deep granite fractures. Nat. Commun. 8, 55.
Eeva, S., Karjalainen, A., Koivisto, E., Korkka-Niemi, K., Rautio, A., Räisänen, O., Gee, R., Birt, B., 2023. Hydrogeological characterization of crystalline bedrock using borehole magnetic resonance. Groundwater 61, 793–815.
Fabritius, O., Fabritius, A., Hellings, M., Sorokina, T., Sojakka, T., Jakobsson, A.M., Li, X., Sammaljärvi, J., Sittari-Kauppi, M., 2024. Radium sorption on crystalline rock; spatial distribution and sorption modeling study. Appl. Geochem. 162, 105930.
Fernandes, M.M., Klinkenberg, M., Baeyens, B., Bosbach, D., Brandt, F., 2023. Adsorption of Ba and ^{226}Ra on illite: a comparative experimental and modelling study. Appl. Geochem. 159, 105815.
Fisher, R.S., 1998. Geologic and geochemical controls on naturally occurring radioactive materials (NORM) in produced water from oil, gas, and geothermal operations. Environ. Geosci. 5, 139–150.
Freeze, G., Stein, E., Brady, P.V., Lopez, C., Sassani, D., 2019. Deep borehole disposal safety case. Sandia National Laboratories Report SAND2019-1915, Albuquerque, NM, p. 94.
Fritz, P., Frape, S.K., Drimmie, R.J., Appleyard, E.C., Hattori, K., 1994. Sulfate in brines in the crystalline rocks of the Canadian Shield. Geochim. Cosmochim. Acta 58, 57–65.
Fox, A., Forchhammer, K., Pettersson, A., La Pointe, P.L., Lim, D.-H., 2012. Geological discrete fracture network model for the Olkiluoto Site, Eurajoki, Finland. Version 2.0. POSIVA 2012-27, POSIVA PY: Eurajoki, Finland.
Gaucher, E.C., Blanc, P., 2006. Cement/clay interactions – a review: experiments, natural analogues and modeling. Waste Manag. 26, 776–788.
Grandia, F., Merino, J., Bruno, J., 2008. Assessment of the radium-barium co-precipitation and its potential influence on the solubility of Ra in the near-field. SKB Technical Report TR-08-07, Swedish Nuclear Fuel and Waste Management Co, Stockholm, Sweden.
Glynn, P., Reardon, E.J., Plummer, L.N., Busenberg, E., 1990. Reaction paths and equilibrium end-points in solid-solution aqueous-solution systems. Geochim. Cosmochim. Acta 54, 267–282.
Glynn, P., 2000. Solid-solution solubilities and thermodynamics: sulfates, carbonates and halides. Rev. Min. Geochem. 40, 481–511.
Hammond, G.E., Lichtner, P.C., Mills, R.T., 2013. Evaluating the performance of parallel subsurface simulators: an illustrative example with PFLOTRAN. Water Resour. Res. 50, 208–228.
Hartley, L., Cox, I., Holton, D., Hunter, F., Joyce, S., Gylling, B., Lindgren, M., 2004. Groundwater flow and radionuclide transport modelling using CONNECTFLOW in support of the SR Can assessment. SKB report R-04-61, Swedish Nuclear Fuel and Waste Management Co, Stockholm, Sweden.
Heberling, F., Metz, V., Böttle, M., Curti, E., Geckeis, H., 2018. Barite recrystallization in the presence of ^{226}Ra and ^{133}Ba. Geochim. Cosmochim. Acta 232, 124–139.
Hedin, A., Olsson, O., 2016. Crystalline rock as a repository for swedish spent nuclear fuel. Elements 12, 247–252.
Hedström, H., Ramebäck, H., Ekberg, C., 2013. A study of the Arrhenius behavior of the co-precipitation of radium, barium and strontium sulfate. J. Radioanal. Nucl. Chem. 298, 847–852.
Hyman, J.D., Gabel, C.W., Painter, S.L., Makedonska, N., 2014. Conforming delaunay triangulation of stochastically generated three dimensional discrete fracture networks: a fracture rejection algorithm for meshing strategy. SIAM J. Sci. Comput. 36, 1871–1894.
Hyman, J.D., Karra, S., Makedonska, N., Gable, C.W., Painter, S.L., Viswanathan, H.S., 2015. DFNWORKS: a discrete fracture network framework for modeling subsurface flow and transport. Comput. Geosci. 84, 10–19.
Hyman, J.D., Navarre-Sitchler, A., Sweeney, M.R., Pachalieva, A., Carey, J.W., Viswanathan, H.S., 2024. Quartz dissolution effects on flow channelization and transport behavior in three-dimensional fracture networks. Geochem. Geophys. Geosyst. 25, e2024GC011550.
IAEA, 2003. Extent of environmental contamination by Naturally Occurring Radioactive Material (NORM) and technological options for mitigation. In Technical Reports Series (ed. I.A.E Agency). International Atomic Energy Agency, Vienna.
Jirásek, J., Matýsek, D., Alexa, P., Osovský, M., Uhlář, R., Sivek, M., 2020. High specific activity of radium isotopes in baryte from the Czech Part of the Upper Silesian Basin – an example of spontaneous mine water treatment. Minerals 2020 (10), 103.
Johnson, J.W., Oelkers, E.H., Helgeson, H.C., 1992. SUPCRT92: a software package for calculating the standard molal thermodynamic properties of minerals, gases, aqueous species, and reactions from 1 to 5000 bar and 0 to 1000°C. Comput. Geosci. 18, 899–947.
Kersten, M., 2025. Aqueous solubilities in the apatite solid-solution system with double co-substitution on both Ca-Sr cation and OH-F anion sublattice positions. Appl. Geochem. 183, 106323.
Klinkenberg, M., Brandt, F., Breuer, U., Bosbach, D., 2014. Uptake of Ra during the recrystallization of barite: a microscopic and time of flight-secondary ion mass spectrometry study. Environ. Sci. Technol. 48, 6620–6627.
Klinkenberg, M., Werber, J., Barthel, J., Vinograd, V., Poonoosamy, J., Kruth, M., Bosbach, D., Brandt, F., 2018. The solid solution-aqueous solution system (Sr, Ba, Ra)SO_4+H_2O: a combined experimental and theoretical study of phase equilibria at Sr-rich compositions. Chem. Geol. 497, 1–17.
Konrad-Schmolke, M., Halama, R., Wirth, R., Thomen, A., Klitscher, N., Morales, L., Schreiber, A., Wilke, F.D.H., 2018. Mineral dissolution and reprecipitation mediated by an amorphous phase. Nat. Commun. 2018 (9), 1637.
Kosakowski, G., Watanabe, N., 2014. OpenGeosys-Gem: a numerical tool for calculating geochemical and porosity changes in saturated and partially saturated media. Phys. Chem. Earth 70–71, 138–149.
Kulik, D.A., Wagner, T., Dmytrieva, S.V., Kosakowski, G., Hingerl, F., Chudnenko, K.V., Berner, U.R., 2013. GEM-Selektor geochemical modeling package: revised algorithm and GEMS3K numerical kernel for coupled simulation codes. Comput. Geosci. 17, 1–24.
Langmuir, D., Riese, A.C., 1985. The thermodynamic properties of radium. Geochim. Cosmochim. Acta 49, 1593–1601.
Langmuir, D., 1997. Aqueous Environmental Geochemistry. Prentice Hall, Upper Saddle River, NJ, p. 600.
Lichtner, P.C., Carey, J.W., 2006. Incorporating solid solutions in reactive transport equations using a kinetic discrete-composition approach. Geochim. Cosmochim. Acta 70, 1356–1378.
Lichtner, P.C., Hammond, G.E., Lu, C., Karra, S., Bisht, G., Andre, B., Mills, R., Kumar, J., 2015. PFLOTRAN user manual: a massively parallel reactive flow and transport model for describing surface and subsurface processes. In: Los Alamos National Lab. (LANL), Los Alamos, NM (United States); Sandia.
Liu, D.J., Hendry, M.J., 2011. Controls on Ra-226 during raffinate neutralization at the Key Lake uranium mill, Saskatchewan, Canada. Appl. Geochem. 26, 2113–2120.
Liu, S., Jacques, D., 2017. Coupled reactive transport model study of pore-size effects on solubility during cement-bicarbonate water interaction. Chem. Geol. 466, 588–599.
MacQuarrie, K.T.B., Mayer, K.U., 2005. Reactive transport modeling in fractured rock: a state-of-the-science review. Earth Sci. Rev. 72, 189–227.
Marty, N.C.M., Tournassat, C., Burnol, A., Giffaut, E., Gaucher, E.C., 2009. Influence of reaction kinetics and mesh refinement on the numerical modelling of concrete/clay interactions. J. Hydrol. 364, 58–72.
Molins, S., Knabner, P., 2019. Multiscale approaches in reactive transport modeling. Rev. Min. Geochem. 85, 27–48.
Nagra, 2002. Models, codes, and data for safety assessment. Nagra Technical Report 02-06, Wettingen, Switzerland, p. 504.
Parkhurst, D.L., Appelo, C.A.J., 1999. User's guide to PHREEQC (Version 2)—A computer program for speciation, batch-reaction, one-dimensional transport, and inverse geochemical calculations. U.S. Geological Survey Water-Resources Investigations Report 99-4259, 312 p.
Phillips, E.J.P., Landa, E.R., Kraemer, T.F., Zielinski, R.A., 2001. Sulfate-reducing bacteria release barium and radium from naturally occurring radioactive material in oil-field barite. Geomicrobiol J. 18, 167–182.
Poonoosamy, J., Obaied, A., Deissmann, G., Prasianakis, N.I., Kindelmann, M., Wollenhaupt, B., Bosbach, D., Curti, E., 2023. Microfluidic investigation of pore-size dependency of barite nucleation. Commun. Chem. 2023 (6), 250.
Poonoosamy, J., Kaspor, A., Schreinemachers, C., Bosbach, D., Cheong, O., Kowalski, P. M., Obaied, A., 2024. A radiochemical lab-on-a-chip paired with computer vision to unlock the crystallization kinetics of (Ba,Ra)SO_4. Sci. Rep. 2024 (14), 9502.
Prieto, M., 2009. Thermodynamics of solid solution-aqueous solution systems. Rev. Min. Geochem. 70, 47–85.
Putnis, A., 2009. Mineral replacement reactions. Rev. Min. Geochem. 70, 87–124.
Reed, M., 1982. Calculation of multicomponent chemical equilibria and reaction processes in systems involving minerals, gases and an aqueous phase. Geochim. Cosmochim. Acta 46, 513–528.
Rollinson, H., Pease, V., 2021. Using Geochemical Data: To Understand Geological Processes, second ed. Cambridge University Press, Cambridge, UK. p. 346.
Rosenberg, Y.O., Sadeh, Y., Metz, V., Pina, C.M., Ganor, J., 2014. Nucleation and growth kinetics of $Ra_xBa_{1-x}SO_4$ solid solution in NaCl aqueous solutions. Geochim. Cosmochim. Acta 125, 290–307.

Rosenberg, Y.O., Sade, Z., Ganor, J., 2018. The precipitation of gypsum, celestine, and Ba sulfates and co-precipitation of radium during seawater evaporation. Geochim. Cosmochim. Acta 233, 50–65.
Roubinet, D., de Dreuzy, J.R., Tartakovsky, D.M., 2012. Semi-analytical solutions for solute transport and exchange in fractured porous media. Water Resour. Res. 48, W01542.
Rudin, S., Kowalski, P.M., Klinkenberg, M., Bosbach, D., Brandt, F., 2024. Anisotropy of barite during crystal growth and the uptake of radium. Cryst. Growth Des. 24, 7774–7788.
Ruiz-Agudo, E., Putnis, C.V., Putnis, A., 2014. Coupled dissolution and precipitation at mineral-fluid interfaces. Chem. Geol. 383, 132–146.
Scibek, J., Kubo, T., Koike, K., Achtziger-Zupančič, 2025. Permeability of granitic drill core tested by steady flow and transient flow gas permeameter probes: improvements to methods and applications. Eng. Geol. 351, 108023.
Schild, M., Siegesmund, S., Vollbrecht, A., Mazurek, M., 2001. Characterization of granite matrix porosity and pore-space geometry by in situ and laboratory methods. Geophys. J. Int. 146, 111–125.
Seigneur, N., Mayer, K.U., Steefel, C.I., 2019. Reactive transport in evolving porous media. Rev. Min. Geochem. 85, 197–238.
Shao, H., Dmytrieva, S.V., Kolditz, O., Kulik, D.A., Pfingsten, W., Kosakowski, G., 2009. Modeling reactive transport in non-ideal aqueous solid-solution system. Appl. Geochem. 24, 1287–1300.
SKB, 2011. Long-term safety for the final repository for spent nuclear fuel at Forsmark. SKB Technical Report TR-11-01, Swedish Nuclear and Waste Management Co, Stockholm, Sweden, p. 893.
Steefel, C.I., Van Cappellen, P., 1990. A new kinetic approach to modeling water-rock interaction: the role of nucleation, precursors and Ostwald ripening. Geochim. Cosmochim. Acta 54, 2657–2677.
Steefel, C.I., DePaolo, D.J., Lichtner, P.C., 2005. Reactive transport modeling: an essential tool and a new research approach for the Earth sciences. Earth Planet. Sci. Lett. 240, 539–558.
Steefel, C.I., Appelo, C.A.J., Arora, B., Jacques, D., Kalbacher, T., Kolditz, O., Lagneau, V., Lichtner, P.C., Mayer, K.U., Meeussen, J.C.L., Molins, S., Moulton, D., Shao, H., Šimůnek, J., Spycher, N., Yabusaki, S.B., Yeh, G.T., 2015. Reactive transport codes for subsurface environmental simulations. Comput. Geosci. 19, 445–478.
Steefel, C.I., Hu, M., 2022. Reactive transport modeling of mineral precipitation and carbon trapping in discrete fracture networks. Water Resour. Res. 58, e2022WR032321.
Sweeney, M.R., Gable, C.W., Karra, S., Stauffer, P.H., Pawar, R.J., Hyman, J.D., 2020. Upscaled discrete fracture matrix model (UDFM): an octree-refined continuum representation of fractured porous media. Comput. Geosci. 24, 293–310.
Tesoriero, A.J., Pankow, J.F., 1996. Solid solution portioning of Sr^{2+}, Ba^{2+}, and Cd^{2+} to calcite. Geochim. Cosmochim. Acta 60, 1053–1063.
Tournassat, C., Grangeon, S., Leroy, P., Giffaut, E., 2013. Modeling specific pH dependent sorption of divalent metals on montmorillonite surfaces. A review of pitfalls, recent achievements and current challenges. Am. J. Sci. 313, 395–451.
Tsang, C.F., Neretnieks, I., Tsang, Y., 2015. Hydrologic issues associated with nuclear waste repositories. Water Resour. Res. 51, 6923–6972.
Tutolo, B.M., Leong, J.A., 2025. Serpentine solid solutions and hydrogen production on Early Earth and Mars. Elements 21, 177–183.
Tullborg, E., Larson, S., 2006. Porosity in crystalline rocks – a matter of scale. Eng. Geol. 84, 75–83.
Ulrych, J., Adamovic, J., Zak, K., Frana, J., Randa, Z., Langrova, A., Skala, R., Chvatal, M., 2007. Cenozoic "radiobarite" occurrences in the Ohre (Eger) Rift, Bohemian Massif: mineralogical and geochemical revision. Geochemistry 67, 301–312.
Vinograd, V.L., Brandt, F., Rozov, K., Klinkenberg, M., Refson, K., Winkler, B., Bosbach, D., 2013. Solid-aqueous equilibrium in the $BaSO_4$-$RaSO_4$-H_2O system: first-principles calculations and a thermodynamic assessment. Geochim. Cosmochim. Acta 122, 398–417.
Vinograd, V.L., Kulik, D.A., Brandt, F., Klinkenberg, M., Weber, J., Winkler, B., Bosbach, D., 2018. Thermodynamics of the solid solution – Aqueous solution system $(Ba,Sr,Ra)SO_4 + H_2O$: I. The effect of strontium content on radium uptake by barite. Appl. Geochem. 89, 59–74.
Viswanathan, H.S., Ajo-Franklin, J., Birkholzer, J.T., Carey, J.W., Guglielmi, Y., Hyman, J.D., Karra, S., Pyrak-Nolte, L.J., Rajaram, H., Srinivasan, G., Tartakovsky, D.M., 2021. From fluid flow to coupled processes in fractured rock: recent advances and new frontiers. Rev. Geophys. 60, e2021RG000744.
Wang, Y., Chi, G., Li, Z., Bosman, S., 2021. Large-scale thermal convection in sedimentary basins revealed by coupled quartz cementation-dissolution distribution pattern and reactive transport modeling – a case study of the Proterozoic Athabasca Basin. Earth Planet. Sci. Lett. 574, 117168.
Wang, Y., Chi, G., 2023. Coupling of thermal convection and basin-basement fluid mixing is critical for the formation of unconformity-related uranium deposits: insights from reactive transport modeling. Chem. Geol. 641, 121764.
Wang, Y., Chi, G., Ferguson, D., McKee, K., Anderson, M., Robbins, J., 2024. Geochemical modeling of U-Ni-Co-As transport and deposition in acidic basinal brines: implications for unconformity-related U-(Ni-Co-As) mineralization in the Athabasca Basin (Canada). Chem. Geol. 670, 122456.
Wang, Y., Chi, G., Bosman, S.A., 2025. Basin-scale production of hyperacidic brines is critical for the formation of high-grade and large-tonnage uranium deposits in sedimentary basins. Geochim. Cosmochim. Acta 397, 1–12.
Weber, J., Barthel, J., Brandt, F., Klinkenberg, M., Breuer, U., Kruth, M., Bosbach, D., 2016. Nano-structural features of barite crystals observed by electron microscopy and atom probe tomography. Chem. Geol. 424, 51–59.
Weber, J., Barthel, J., Klinkenberg, M., Bosbach, D., Kruth, M., Brandt, F., 2017. Retention of ^{226}Ra by barite: the role of internal porosity. Chem. Geol. 466, 722–732.
White, W.M., 2020. Geochemistry, second ed. John Wiley & Sons, p. 960.
Wind, S.C., Hannington, M.D., Schneider, D.A., Fietzke, J., Kilias, S.P., Gemmell, B., 2023. Origin of hydrothermal barite in polymetallic veins and carbonate-hosted deposit of the Cyclades Continental Back Arc. Econ. Geol. 118, 1959–1994.
Yang, Y., Churakov, S.V., Patel, R.A., Prasianakis, N., Deissmann, G., Bosbach, D., Poonoosamy, J., 2024. Pore-scale modeling of water and ion diffusion in partially saturated clays. Water Resour. Res. 60, e2023WR035595.
Zhang, X., Ma, F., Dai, Z., Wang, J., Chen, J., Ling, H., Soltanian, M.R., 2022. Radionuclide transport in multi-scale fractured rocks: a review. J. Hazard. Mater. 424, 127550.
Zhang, T., Gregory, K., Hammack, R.W., Vidic, R.D., 2014. Co-precipitation of radium with barium and strontium sulfate and its impact on the fate of radium during treatment of produced water from unconventional gas extraction. Environ. Sci. Technol. 48, 4596–4603.
Zhang, Z., Yi, L., Nie, Z., 2025. Co-precipitation of radium in high-salinity environments: implications from laboratory experiments and field surveys. Chem. Geol. 672, 122506.
Zhang, Q., Deng, H., Dong, Y., 2026. The impacts of well-connected intragranular porosity on mineral dissolution rates. Geochim. Cosmochim. Acta 412, 1–17.
Zhu, C., 2004. Coprecipitaiton in the barite isostructural family: 2. Numerical simulations of reactions and mass transport. Geochim. Cosmochim. Acta 68, 3339–3349.
Zuber, A., Motyka, J., 1994. Matrix porosity as the most important parameter of fissured rocks for solute transport at large scales. J. Hydrol. 158, 19–46.